**Key Points:**
- The seasonal drivers in carbonate system parameters are decomposed and their relative importance determined
- SOCCOM climatology matches existing climatology well in the Subtropics and less so in more poleward zones and during winter
- Float-based climatologies suggest an increase in carbon- and nutrient-rich upwelled waters south of the Subantarctic Front

**Supporting Information:**
- Supporting Information S1
- Table S1

**Correspondence to:**
N. L. Williams,
nancy.williams@noaa.gov

# Assessment of the Carbonate Chemistry Seasonal Cycles in the Southern Ocean From Persistent Observational Platforms

N. L. Williams[1,2] (ID), L. W. Juranek[1] (ID), R. A. Feely[3], J. L. Russell[4] (ID), K. S. Johnson[5] (ID), and B. Hales[1]

[1]College of Earth, Ocean, and Atmospheric Sciences, Oregon State University, Corvallis, OR, USA, [2]Pacific Marine Environmental Laboratory, NOAA, Seattle, WA, USA, [3]Pacific Marine Environmental Laboratory, National Oceanic and Atmospheric Administration, Seattle, WA, USA, [4]Department of Geosciences, University of Arizona, Tucson, AZ, USA, [5]Monterey Bay Aquarium Research Institute, Moss Landing, CA, USA

**Abstract** Observations from Southern Ocean Carbon and Climate Observations and Modeling (SOCCOM) biogeochemical profiling Argo floats are used to characterize the climatological seasonal cycles and drivers of dissolved inorganic carbon, total alkalinity, pH, the partial pressure of carbon dioxide ($CO_2$), and the saturation state of aragonite at the surface and at 200 m across five Southern Ocean frontal regimes, including under sea ice. The Southern Ocean ranges from a temperature-dominated system in the northernmost Subtropical Zone to a biologically dominated system in the most poleward Seasonal Sea Ice Zone. In all zones, the ingassing or outgassing of $CO_2$ must be balanced by geostrophic and Ekman transport, mixing from below, and particle transport of carbon into or out of the euphotic zone. The climatological seasonal cycles spanning the period from 2014 to 2017 compare favorably with existing climatologies in spring and summer and less so during winter months, at higher latitudes, and in ice-covered regions due, in part, to limited wintertime observations before SOCCOM. We observe increases in the carbon and nutrient content of surface waters south of the Subantarctic Front between climatological data products and the SOCCOM float climatologies, even after adjusting for anthropogenic change, suggesting a large-scale increase in the amount of upwelled carbon- and nutrient-rich deep waters. This increased upwelling corresponds to a positive Southern Annular Mode Index over 2014–2017 and likely acts to decrease the magnitude of the Southern Ocean sink of total carbon by increasing outgassing of natural $CO_2$, especially during winter months.

**Plain Language Summary** Observations from robotic floats deployed as part of the Southern Ocean Carbon and Climate Observations and Modeling project are used to characterize the seasonal cycle of carbon dioxide in the Southern Ocean. In the Subtropical Zone, temperature controls the seasonal cycles, but in the more southern zones, biological processes are dominant. Some zones give off carbon dioxide to the atmosphere on average, while other zones take up carbon dioxide on average. This gain or loss of carbon dioxide is balanced in each zone by other processes such as transport of water masses with different properties in or out of the zone, sinking of biological particles, or mixing with deeper waters. We compare the Southern Ocean Carbon and Climate Observations and Modeling observations with an existing data set for the Southern Ocean, and they match well in the northernmost zones but there are discrepancies to the south. Specifically, we observe increased surface ocean carbon dioxide and increased acidity relative to the earlier data set in the Antarctic Circumpolar Current and farther south. This may be due to increased mixing accompanying the stronger winds that have been observed between 2014 and 2017. The difference may also be due, in part, to undersampling in wintertime in the earlier data set.

## 1. Introduction

As concentrations of carbon dioxide ($CO_2$) increase in Earth's atmosphere due to continued fossil fuel burning, cement production, and land use changes, the ocean continues to play a major role in mediating this increase by absorbing about one quarter of this anthropogenic $CO_2$ (Le Quéré et al., 2016). This $CO_2$ uptake, known as the ocean carbon sink, is highly variable both spatially and temporally. The Southern Ocean south of 30°S makes up just 30% of the ocean's surface, yet it accounts for approximately 43% of the total ocean anthropogenic $CO_2$ sink (Frölicher et al., 2015). As nations move toward quantifying the sources and sinks of anthropogenic $CO_2$, it is important to understand the mechanisms responsible for this uptake and how we can expect them to change in the future.

The direction of the flux of $CO_2$ between the ocean and the atmosphere, $F$, is driven by the gradient in the partial pressure of $CO_2$ ($pCO_2$) between the ocean and the atmosphere. The magnitude of $F$ depends on wind speed and the solubility of $CO_2$ as a function of seawater temperature and salinity. Several high-quality flux products have been developed to constrain $F$ regionally and globally by compiling existing observations and interpolation and neural network approaches (Landschützer et al., 2013; Takahashi et al., 2014, hereafter referred to as T14; Wanninkhof et al., 2013). These flux products incorporate the highest quality $pCO_2$ data and are carefully compiled. Nonetheless, in regions such as the Southern Ocean where wintertime conditions are unfavorable for sampling, they are and biased toward summer months. Williams et al. (2017) found that new observations from Southern Ocean Carbon and Climate Observations and Modeling (SOCCOM) biogeochemical Argo profiling floats indicate higher wintertime surface ocean $pCO_2$ in the Antarctic Circumpolar Current (ACC) and in seasonally sea ice-covered waters than any data product to date, a difference which could have large implications for the global carbon budget. This observed difference between SOCCOM and previous data sets is not surprising given that before SOCCOM there were limited Southern Ocean wintertime observations, but it is important to distinguish the origin of this difference. Surface ocean $pCO_2$ is controlled by a variety of factors ranging from the carbon content and alkalinity of the seawater to the sea surface temperature ($T$) and the rate of gas exchange with the atmosphere. The carbon content and alkalinity are controlled, to a first order, by the large-scale circulation of the ocean, with local processes such as biological production, calcification, and sea ice melt/refreeze asserting seasonal controls.

Few fully resolved annual cycles in carbonate system chemistry exist for the Southern Ocean (Munro et al., 2015; T14) and even the most realistic Earth system models tend to both be biased (Law et al., 2017; Rickard et al., 2016) and to underestimate the seasonal cycles in carbonate system parameters (Sasse et al., 2015) as compared to recent observational time series data. This is because data sets that do exist are often biased toward summer and coastal data (Jones et al., 2017; McNeil et al., 2011; Roden et al., 2013, 2016; Shadwick et al., 2013) or are heavily weighted toward data from the Drake Passage region (Munro et al., 2015; Sprintall et al., 2012). These Earth system models form the basis upon which predictions of future climate are made, and misrepresentations of the current state of the ocean can lead to biases when projected into the future. For example, Sasse et al. (2015) found that accounting for seasonality in the carbonate system advances the initial onset of month-long aragonite (calcium carbonate) undersaturation by $17 \pm 10$ years. It is therefore important to understand the current seasonal cycles and drivers of the ocean carbon system if Earth system models are to be useful for such projections.

Recent developments in ocean observing, such as the addition of biogeochemical sensors to Argo floats that sample between the surface and 1,800 m at 10-day intervals, have provided the opportunity for unprecedented sampling in remote regions such as the Southern Ocean. Here we use this newly available surface and subsurface biogeochemical float data to examine the seasonal variability in the carbonate system and its drivers across five major frontal zones of the open Southern Ocean. We then create climatological seasonal cycles for total alkalinity (TA), dissolved inorganic carbon (DIC), pH, $pCO_2$, and the saturation states of aragonite and calcite ($\Omega_{Ar}$ and $\Omega_{Ca}$, respectively), as well as $T$, salinity (S), and nitrate ($NO_3^-$), and compare them with the existing T14 climatology.

## 2. Physical Setting

The bulk of the Southern Ocean south of 30°S can be divided into five zones defined by the locations of the subtropical front, subantarctic front, polar front, and the southern boundary of the ACC (Orsi et al., 1995). All floats used in this study were divided into one of these five zones: Subtropical Zone (STZ), Subantarctic Zone (SAZ), Polar Frontal Zone (PFZ), Antarctic Southern Zone (ASZ), and Seasonal Sea Ice Zone (SSIZ). The STZ is the most equatorward of the five zones and is characterized by warm, low-$NO_3^-$ ($<5$ μmol/kg) surface waters north of the subtropical front. Between the subtropical front and the subantarctic front is the SAZ characterized by elevated $NO_3^-$ ($>5$ μmol/kg), deep winter mixed layers ($>200$ m), and an oxygen minimum near 1,400-m depth (Orsi et al., 1995). South of the subantarctic front and into the eastward flowing ACC is the PFZ where sloping isopycnals bring old carbon- and nutrient-rich deep waters closer to the surface with an oxygen minimum/DIC maximum around 1,000 m (Orsi et al., 1995). South of the polar front are the Antarctic Zone and the Southern Zone, characterized by colder and fresher surface waters, shallower
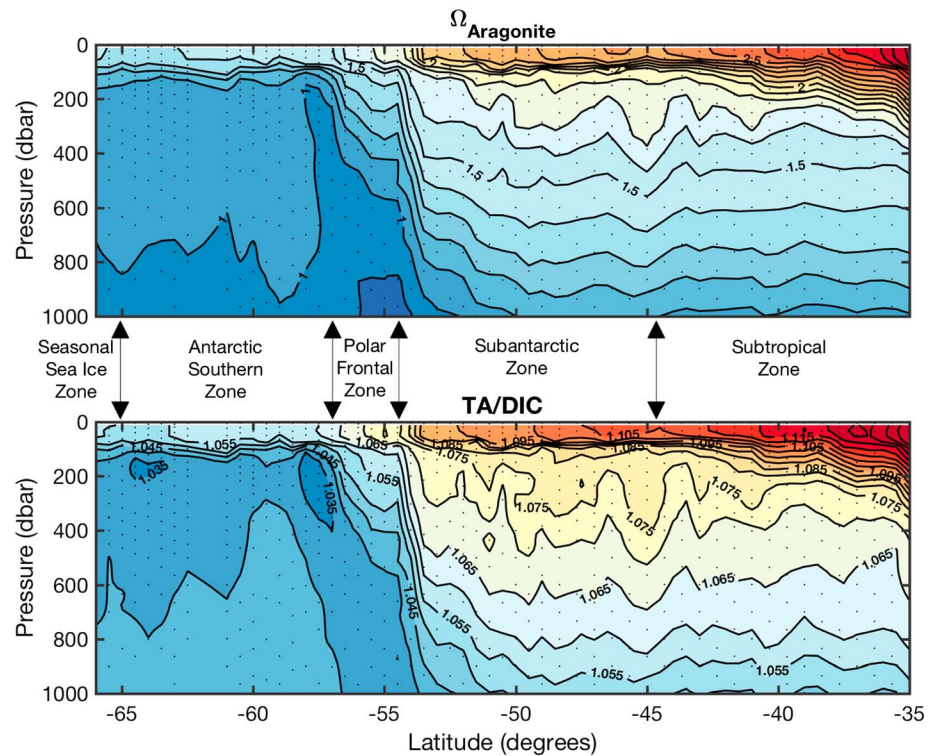
**Figure 1.** Vertical sections of $\Omega_{Ar}$ (top) calculated from bottle samples of total alkalinity and pH (black dots) and total alkalinity (TA)/dissolved inorganic carbon (DIC; bottom) along P16S GO-SHIP repeat hydrographic transect at 150°W in the South Pacific.

winter mixed layers (~100 m), and carbon- and nutrient-rich oxygen minimum waters shoaling to between 400 and 700 m (Orsi et al., 1995). For the purposes of this study, the Antarctic Zone (between the polar front and the Southern ACC front) and Southern Zone (between the Southern ACC front of the ACC and the Southern boundary of the ACC) will be combined into the ASZ. The most poleward zone is the SSIZ, which is similar to the ASZ with the main difference being that it is covered with sea ice during some portion of the year. Williams et al. (2017) combined the PFZ and the ASZ into one zone called the Polar Antarctic Zone because of similarities in the seasonal cycle in $pCO_2$, but for the purposes of this study, it is important to examine the drivers and climatological values in the PFZ and ASZ separately.

The large-scale circulation of the Southern Ocean brings old carbon-rich deep waters to the surface, creating very low aragonite calcium carbonate saturation states ($\Omega_{Ar}$) near the surface in the PFZ, ASZ, and the SSIZ and allowing natural $CO_2$ to outgas into the atmosphere. This pattern is evident in Figure 1, which shows the $\Omega_{Ar}$ (calculated from bottle samples of pH and TA shown as black dots) and TA/DIC between the surface and 1,000 m along the P16S GO-SHIP repeat hydrographic line (Talley et al., 2015) meridional transect along 150°W.

## 3. Methods

### 3.1. Float Data

Water column measurements of T, S, P, oxygen ($O_2$), $NO_3^-$, and in situ pH on the total scale were collected at 10-day intervals on SOCCOM floats throughout the Southern Ocean. Data over the period 2014–2018 for 39 floats (Table 1) were analyzed for this study, and the quality-controlled data set is archived and available for download at http://doi.org/10.6075/J0PG1PX7 as *Snapshot 2018-03-06*. There were 91 active SOCCOM floats as of 14 December 2017, but only the subset of floats with quality-controlled pH data is used for this study. All SOCCOM float data were quality controlled as described in Johnson et al. (2017), which also summarizes the fleet-wide sensor performance. Figure 2 shows a map of the floats used in this study colored by zone and

**Table 1**
*Floats Used in This Study*

| Frontal region | UW ID | WMO ID | Deployment date | Cruise ID |
|---|---|---|---|---|
| Subtropical Zone | 9254 | 5904395 | 21 April 2014 | P16S |
| | 9101 | 5904187 | 18 April 2014 | P16S |
| | 9313 | 5904474 | 12 December 2014 | A12 |
| | 9749 | 5904675 | 12 January 2016 | HEOBI |
| | 9630 | 5904674 | 30 May 2016 | P15S |
| | 9744 | 5904678 | 6 April 2016 | Eddy |
| Subantarctic Zone | 9031 | 5904396 | 11 April 2014 | P16S |
| | 9095 | 5904188 | 14 April 2014 | P16S |
| | 8514 | 5904470 | 23 March 2015 | SOTS |
| | 9668 | 5904663 | 8 December 2015 | OOISO |
| | 9646 | 5904661 | 28 December 2015 | OOISO |
| | 9655 | 5904658 | 8 January 2016 | SR1B |
| | 9637 | 5904682 | 1 March 2016 | I8S |
| | 9631 | 5904677 | 31 March 2016 | Eddy |
| | 9632 | 5904763 | 18 May 2016 | P15S |
| | 9634 | 5904693 | 19 May 2016 | P15S |
| | 12575 | 5904854 | 27 December 2016 | HazMat |
| | 9642 | 5904685 | 8 January 2017 | P18 |
| | 12382 | 5904841 | 12 January 2017 | P18 |
| | 12552 | 5904842 | 15 January 2017 | P18 |
| Polar Frontal Zone | 9260 | 5904473 | 27 January 2015 | A12 |
| | 9650 | 5904683 | 3 March 2016 | I8S |
| | 9265 | 5904695 | 13 May 2016 | P15S |
| | 12573 | 5904982 | 27 December 2016 | HazMat |
| Antarctic Southern Zone | 9092 | 5904185 | 7 April 2014 | P16S |
| | 9096 | 5904469 | 10 December 2014 | A12 |
| | 9652 | 5904660 | 7 January 2016 | SR1B |
| | 9657 | 5904659 | 7 January 2016 | SR1B |
| | 9757 | 5904679 | 18 January 2016 | HEOBI |
| | 9602 | 5904684 | 28 February 2016 | I8S |
| | 12545 | 5904856 | 29 December 2016 | HazMat |
| | 12543 | 5904980 | 1 January 2017 | HazMat |
| | 12558 | 5905069 | 11 January 2017 | ACE |
| | 12388 | 5905099 | 16 April 2017 | PIPERS |
| Seasonal Sea Ice Zone | 9091 | 5904184 | 3 April 2014 | P16S |
| | 12381 | 5904857 | 12 January 2017 | HazMat |
| | 9275 | 5904472 | 18 January 2015 | A12 |
| | 9099 | 5904468 | 19 January 2015 | A12 |
| | 9125 | 5904397 | 21 January 2015 | A12 |

their relations to the fronts of the ACC. Some floats occupy multiple zones over their lifetimes, and so data that do not fit the oceanographic description outlined in section 2 for their primary zone listed in Table 1 are discarded. The five floats that will be discussed in most detail in this study are highlighted with black dots along their path and labeled with their UW ID number.

The floats measure pH using a Deep Sea DuraFET pH sensor (Johnson et al., 2016). A second carbonate system parameter, along with T, S, and P, is required in order to fully characterize the carbonate system. In this case, the float-measured pH is combined with an estimate for TA to calculate DIC, $pCO_2$ (Williams et al., 2017), $\Omega_{Ar}$, and $\Omega_{Ca}$. The two TA algorithms used here, LIAR (Locally Interpolated Alkalinity Regression; Carter et al., 2018) and MLR (multiple linear regression; Williams et al., 2017; supporting information), are both based on T, S, P, $O_2$, and location and have uncertainties of 5 and 4.3 $\mu$mol/kg, respectively. The uncertainty in $\Omega_{Ar}$ is estimated to be 0.04 based on the uncertainty of the float pH of 0.01 and the uncertainty of TA of 5 $\mu$mol/kg, with the major contribution of the $\Omega_{Ar}$ uncertainty coming from the float pH sensor. The uncertainty in float-based $\Omega_{Ar}$ is an order of magnitude smaller than the seasonal cycle in surface $\Omega_{Ar}$ in the Southern Ocean and the same order of magnitude as the local annual decrease in $\Omega_{Ar}$ due to anthropogenic carbon increases ($-0.01$ year$^{-1}$; Williams et al., 2015). All carbonate system calculations were performed using CO2SYS for MATLAB
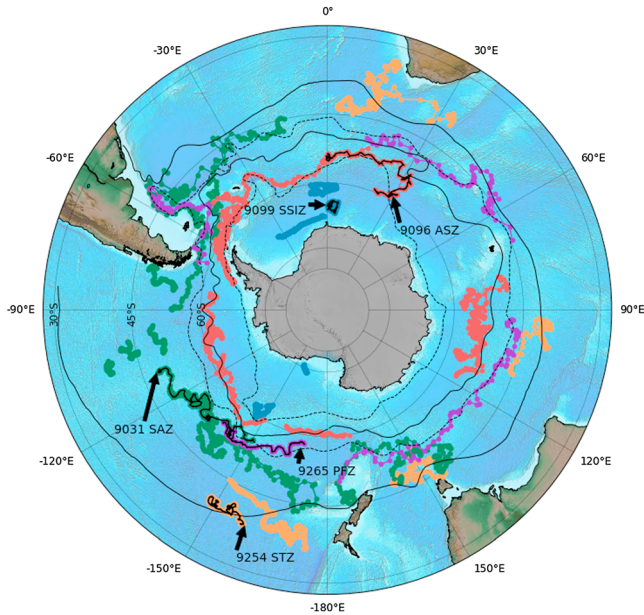
**Figure 2.** A map of float trajectories as of 14 December 2017 with ETOPO1 Global Relief (https://www.ngdc.noaa.gov/mgg/global/global.html) in the background. Each colored dot represents one float profile with the colors distinguishing the five frontal zones. The five floats that will be discussed in most detail in this study are highlighted by black dots along their path and labeled with their UW float ID number. The approximate locations of the Antarctic Circumpolar Current fronts (Orsi et al., 1995) are shown as solid or dashed black lines and from most poleward to most equatorward are Southern boundary of the Antarctic Circumpolar Current (dashed), Polar Front (solid), Subantarctic Front (dashed), and the Subtropical Front (solid).

(van Heuven et al., 2011), the equilibrium constants of Lueker et al. (2000), Dickson (1990), and Perez and Fraga (1987), and the boron/S ratio of Lee et al. (2010) as recommended by A. Dickson (Wanninkhof et al., 2016). For this data set, calculations using the Lee et al. (2010) boron/S ratio result in saturation states on average 1% lower and pH on average 0.004 lower than those calculated using the boron/S ratio of Uppström (1974), which was used in the initial formulations of the Lueker et al. (2000) equilibrium constants (Orr et al., 2015). All pH values are reported at in situ conditions on the total hydrogen ion concentration scale.

### 3.2. Drivers of the Seasonal Cycle

Seasonal changes in carbonate system parameters are driven by a combination of physical and biological drivers, and the relative importance of each driver varies widely across frontal regions. To compare and contrast these regional differences, we decompose these drivers for five representative floats (highlighted with black dots along their trajectories in Figure 2), one from each of the five Southern Ocean frontal zones described in section 2. These specific floats were chosen for their deployment durations and because they carry both pH and nitrate ($NO_3^-$) sensors. We first create budgets for surface $NO_3^-$, DIC, and LIAR TA, and then use those budgets to calculate the contributions of each process to observed changes in pH, $\Omega_{Ar}$, and pCO$_2$. All changes ($\Delta$s) are relative to the first January profile for each float which we call time zero.

We separate the drivers of observed $NO_3^-$ into freshwater fluxes, net community metabolism (NCM), and a residual term:

$$NO_3^- = NO_{3_0}^- + \Delta NO_{3_{freshwater}}^- + \Delta NO_{3_{NCM}}^- + \Delta NO_{3_{residual}}^- \tag{1}$$

TA is also influenced by freshwater, NCM, and a residual term, and is additionally influenced by calcium carbonate ($CaCO_3$) production (calcification) and dissolution:

$$TA = TA_0 + \Delta TA_{freshwater} + \Delta TA_{NCM} + \Delta TA_{CaCO_3} + \Delta TA_{residual} \tag{2}$$

The drivers of DIC are the same as for TA with the addition of gas exchange:

$$DIC = DIC_0 + \Delta DIC_{freshwater} + \Delta DIC_{NCM} + \Delta DIC_{CaCO_3} + \Delta DIC_{gas} + \Delta DIC_{residual} \tag{3}$$

The effects of changes in freshwater are calculated using observed changes in S and the initial ratio of each parameter to S at the surface at time zero:

$$\Delta TA_{freshwater} = \Delta S \cdot \left( \frac{TA_0}{S_0} \right) \tag{4}$$

$$\Delta DIC_{freshwater} = \Delta S \cdot \left( \frac{DIC_0}{S_0} \right) \tag{5}$$

$$\Delta NO_{3_{freshwater}}^- = \Delta S \cdot \left( \frac{NO_{3_0}^-}{S_0} \right) \tag{6}$$

For these relationships to hold we must assume that the freshwater end members (in this case, ice, and precipitation) have concentrations of TA, DIC, and $NO_3^-$ which are zero. We can then solve equation (2) for $\Delta NO_{3_{NCM}}^-$ by assuming that $NO_{3_{residual}}^-$ is zero and the implications of this assumption will be explored in

the discussion. $\Delta TA_{NCM}$ and $\Delta DIC_{NCM}$ can then be calculated from $\Delta N_{NCM}$ by assuming ratios of change of $NO_3^-$:DIC:TA = 16:117: $-16$ during biological production and respiration (Sarmiento & Gruber, 2006):

$$\Delta TA_{NCM} = \Delta NO_{3_{NCM}}^- \cdot \left(\frac{-16}{16}\right) \tag{7}$$

$$\Delta DIC_{NCM} = \Delta NO_{3_{NCM}}^- \cdot \left(\frac{117}{16}\right) \tag{8}$$

It is important to note that the NCM terms are representative of respiration and production occurring in situ, as well as respiration and production that have occurred elsewhere and have been advected, entrained, or mixed into the surface layer over the lifetime of the float. We can then solve equation (3) for $\Delta TA_{CaCO_3}$ by substituting in equations (5) and (8) and assuming that $\Delta TA_{residual}$ is zero. Because the ratio of changes in DIC:TA during calcification is 1:2, we can then calculate $\Delta DIC_{CaCO_3}$:

$$\Delta DIC_{CaCO_3} = 0.5 \cdot \Delta TA_{CaCO_3} \tag{9}$$

To calculate $\Delta DIC_{gas}$, we must calculate $F$ along each float path. To calculate $F$, we first combine the float-measured pH with the algorithm estimate for TA to calculate surface ocean $pCO_2$ as described in Williams et al. (2017). This surface ocean $pCO_2$, combined with estimates for wind speed and atmospheric $CO_2$ values, can be used to calculate the flux of $CO_2$ between the ocean and the atmosphere, $F$:

$$F = kK_0\left(pCO_2^{ocean} - pCO_2^{atmosphere}\right), \tag{10}$$

where $k$ is the gas transfer velocity and $K_0$ is the solubility of $CO_2$ in seawater as a function of T and S. The gas transfer velocity is calculated using the Wanninkhof (2014) wind speed squared parameterization and NCEP (National Centers for Environmental Prediction) reanalysis 6-hourly 10 m winds (Kalnay et al., 1996) and $pCO_2^{atmosphere}$. $pCO_2^{atmosphere}$ is calculated from $xCO_2^{atmosphere}$ obtained from CSIRO Oceans and Atmosphere and the Australian Bureau of Meteorology Cape Grim Baseline Air Pollution Station (https://www.csiro.au/en/Research/OandA/Areas/Assessing-our-climate/Latest-greenhouse-gas-data) corrected for the atmospheric pressure from NCEP reanalysis 6-hourly sea level pressure (Kalnay et al., 1996) and the vapor pressure of water as a function of T and S as described in Dickson et al. (2007). The float $pCO_2$, T, and S data were linearly interpolated from their ~10-day sampling intervals onto 6-hourly time steps, as were the Cape Grim atmospheric $CO_2$ values. $F$ was calculated for each 6-hr window in units of mmol C/m$^2$/day. $F$ at each time is divided by the mixed layer depth in meters (determined as the depth at which density increases by 0.03 kg/m$^3$ relative to the surface density; Dong et al., 2008), by seawater density in kg/m$^3$, and then by four to obtain the change in mixed layer DIC in $\mu$mol/kg$^1$ per 6 hr. The $\Delta DIC_{gas}$ at each float surfacing is then calculated as the cumulative change in mixed layer DIC since time zero. $F$ is decreased by 50% when the float sensed ice to account for decreased air-sea flux through ice. This choice does affect the magnitude of the overall $CO_2$ uptake in the SSIZ but even removing the ice and allowing full gas exchange during winter cannot change the net source/sink status of the SSIZ.

Finally, having calculated $F$, we can solve equation (4) for $\Delta DIC_{residual}$, which represents observed changes in DIC that are not captured in this budget. Because this budget does not explicitly account for physical processes such as horizontal and vertical transport, mixing, or entrainment, $\Delta DIC_{residual}$ is at least partially representative of the effects of these terms as well as artifacts from the errors in the other terms.

We can then calculate the influences of each of the aforementioned processes on pH, $\Omega_{Ar}$, and $pCO_2$ by adding $\Delta DIC$ and $\Delta TA$ to the time zero DIC and TA values, respectively, and holding other variables constant. To calculate the freshwater terms, we also vary S as observed ($\Delta S$). Because pH, $\Omega_{Ar}$, and $pCO_2$ are directly affected by changes in T (whereas $NO_3^-$ and TA are not, and the effects of T on DIC are not instantaneous and are neglected here) we also calculate a separate term to estimate changes in pH, $\Omega_{Ar}$, and $pCO_2$ only due to $\Delta T$. The T terms are calculated by recalculating the time series of pH, $\Omega_{Ar}$, and $pCO_2$ using CO2SYS (van Heuven et al., 2011) over the lifetime of each float starting with the time zero conditions and varying
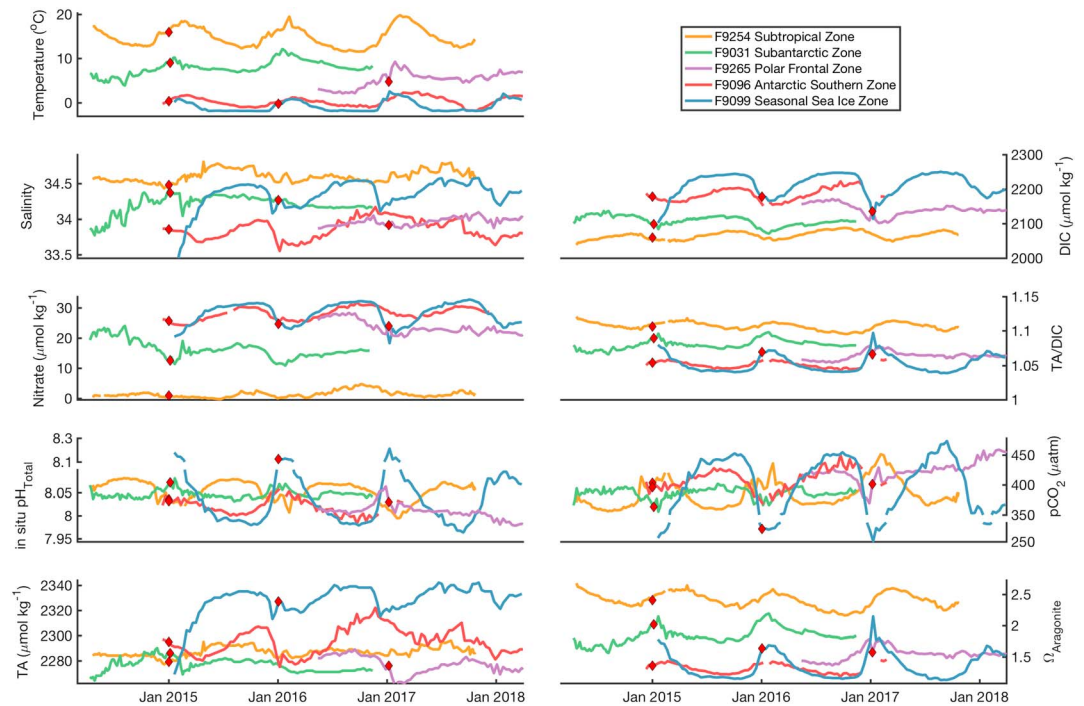
**Figure 3.** Time series of measured (temperature, salinity, nitrate, and pH) and derived quantities (Locally Interpolated Alkalinity Regression [LIAR] total alkalinity [TA], LIAR dissolved inorganic carbon [DIC], LIAR TA/LIAR DIC, LIAR $pCO_2$, and $\Omega_{Ar}$) for each of the five frontal zones with red diamonds denoting time zero for the decomposition analysis.

only T as observed, and then taking the difference with the time zero pH, $\Omega_{Ar}$, and $pCO_2$ values. For example, for pH:

$$\Delta pH_{temperature} = pH(TA_{t0}, DIC_{t0}, S_{t0}, T_t) - pH_{t0} \qquad (11)$$

### 3.3. Float-Based Climatologies

Monthly climatologies of surface and 200-m T, S, $NO_3^-$, in situ $pH_{Total}$, TA, DIC, $pCO_2$, and $\Omega_{Ar}$ were calculated for each of the five Southern Ocean frontal regions using data from 39 floats. We also create separate climatologies for each TA product as well as for DIC and $pCO_2$ calculated from each TA product. To do this, we first create monthly climatologies at the surface and at 200 m for each individual float listed in Table 1. For the surface climatology, the shallowest reading for each profile (~6 m in ice-free conditions and ~20 m under sea ice) is used, and for the 200-m climatology the closest data point to 200 m (±10 m) is used. All float profiles in each calendar month are averaged to create a monthly averaged data product over the lifetime of each float, which contains up to three and a half years of data. Then, all float years for each float are averaged month by month to create a single monthly climatology for each float. All floats in each frontal region are then averaged by month to create a single monthly climatology for each frontal zone. Although pH, DIC, and $\Omega_{Ar}$ are all affected by time-dependent anthropogenic increases in atmospheric $CO_2$, it is appropriate to combine multiple years in this way given that the uncertainty in each of these measured or calculated parameters is greater than or approximately equal to the expected anthropogenic change (T14) over the study period.

### 4. Results

### 4.1. Observed and Derived Quantities

Figure 3 shows the full records of the observed and derived quantities used in the seasonal decompositions of the five representative floats. T decreases from the STZ poleward to the SSIZ, while the amplitude of the seasonal cycle in T also decreases poleward. S is highest in the STZ and decreases poleward until the SSIZ
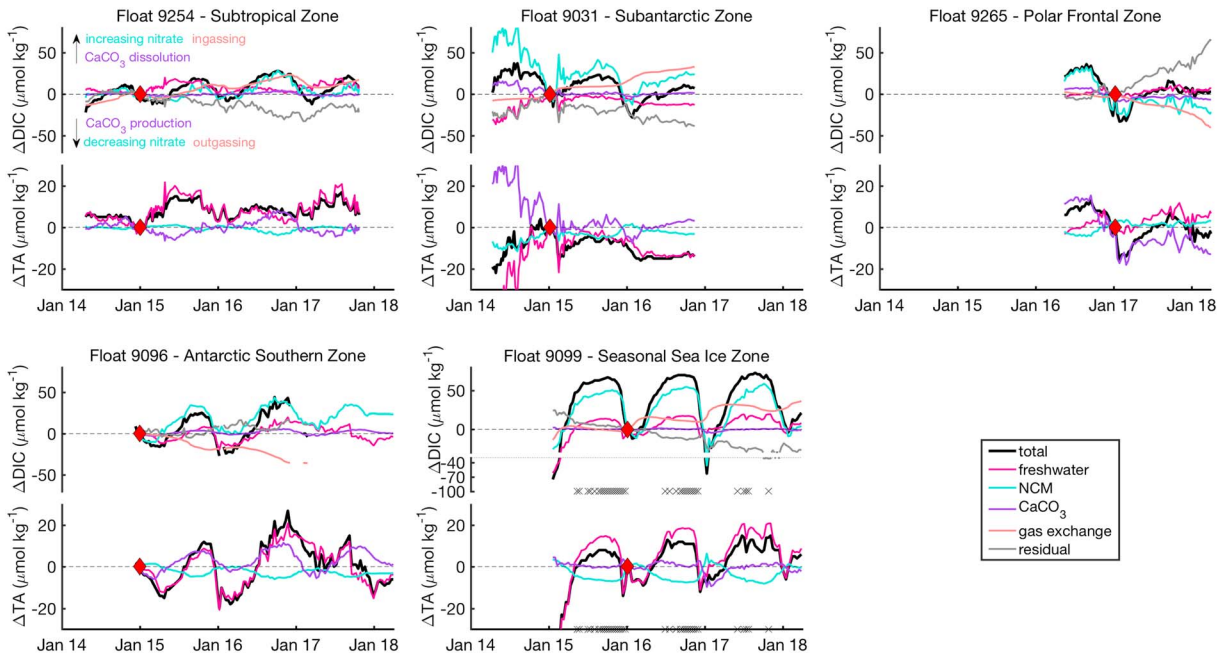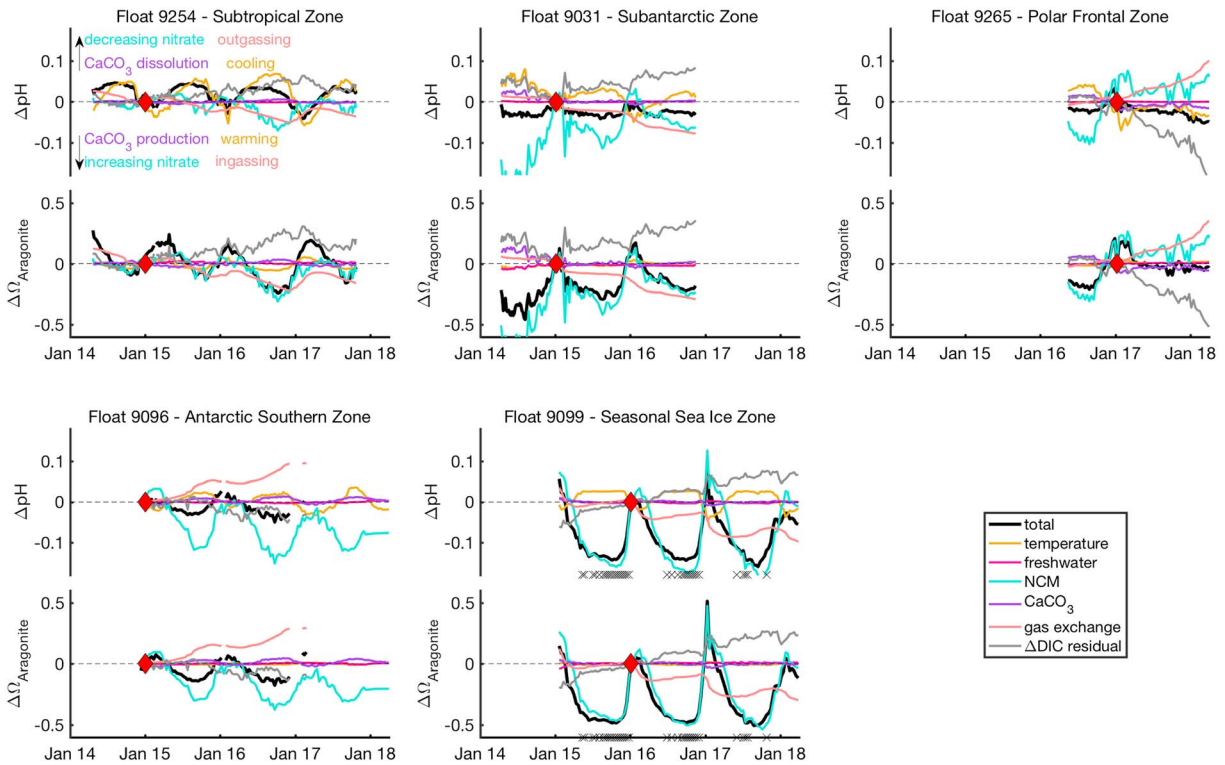
**Figure 4.** Decomposition of the drivers of dissolved inorganic carbon (DIC) and total alkalinity (TA) from five representative floats using the Locally Interpolated Alkalinity Regression TA algorithm. The red diamond in each subplot represents time zero, the black line represents cumulative observed changes in DIC or TA relative to time zero, and the colored lines represent the cumulative contribution of each process to the cumulative observed changes in DIC or TA relative to time zero. Black *crosses* along the *x* axis represent times when Float 9099 sensed sea ice. NCM = net community metabolism.

where brine rejection during sea ice formation and equatorward transport of sea ice causes an overall increase in S and an amplified seasonal cycle in S. $NO_3^-$ and DIC both increase moving poleward reflecting the increasing influence of the old carbon- and nutrient-rich deep waters that are characteristic of this upwelling system as well as persistent micronutrient limitation which prevents complete biological drawdown of $NO_3^-$. TA, which correlates locally with S but is also influenced by biological processes, is highest in the SSIZ and ASZ where high TA waters are upwelled to the surface, and lowest in the PFZ and SAZ where overall net calcification removes TA from the surface and transports it to the deep ocean. $pCO_2$ and pH are inversely related, and their seasonal cycles are strongly influenced by changes in TA and DIC as well as changes in T. The competition between these processes results in a diversity of seasonal cycles for both $pCO_2$ and pH across the five zones. $\Omega_{Ar}$ generally decreases poleward reflecting increasing aqueous $CO_2$ and decreasing carbonate ion concentration. This decrease also corresponds to a decreased buffering capacity (i.e., higher Revelle factor), that is, decreased resistance of changes in seawater $pCO_2$ to changes in DIC. The drivers of the seasonal cycles in all of the carbonate system parameters will be described in the following sections.

### 4.2. Seasonal Drivers of DIC and TA

Figure 4 shows the cumulative observed changes in DIC and TA relative to the first January profile for the five representative floats as well as the cumulative contributions of each process. Both DIC and TA are affected by the addition or removal of freshwater, which manifests as a change in observed S. Seasonal changes in freshwater play only a small role in the SAZ and PFZ and are more significant in the ASZ and the SSIZ where the seasonal melting and formation of sea ice causes seasonal swings in S of ~0.5 for float 9099. S also plays a role in the STZ where a seasonal cycle of evaporation and precipitation is evident. In all zones, the seasonal cycle in DIC is most affected by NCM, then freshwater, and finally, $CaCO_3$ production/dissolution. DIC decreases in spring and summer due to drawdown from primary production and, in the southernmost zones, the addition of freshwater from melting ice. DIC then increases in fall and winter due to respiration and entrainment of higher $NO_3^-$, DIC, and TA waters from below as the mixed layer deepens. For TA, S dominates except for in the PFZ where $\Delta TA_{CaCO3}$ is larger than $\Delta TA_{freshwater}$. NCM is the least important driver for TA, except for in the SAZ, ASZ, and SSIZ where $\Delta TA_{NCM}$ rivals and opposes $\Delta TA_{CaCO3}$.
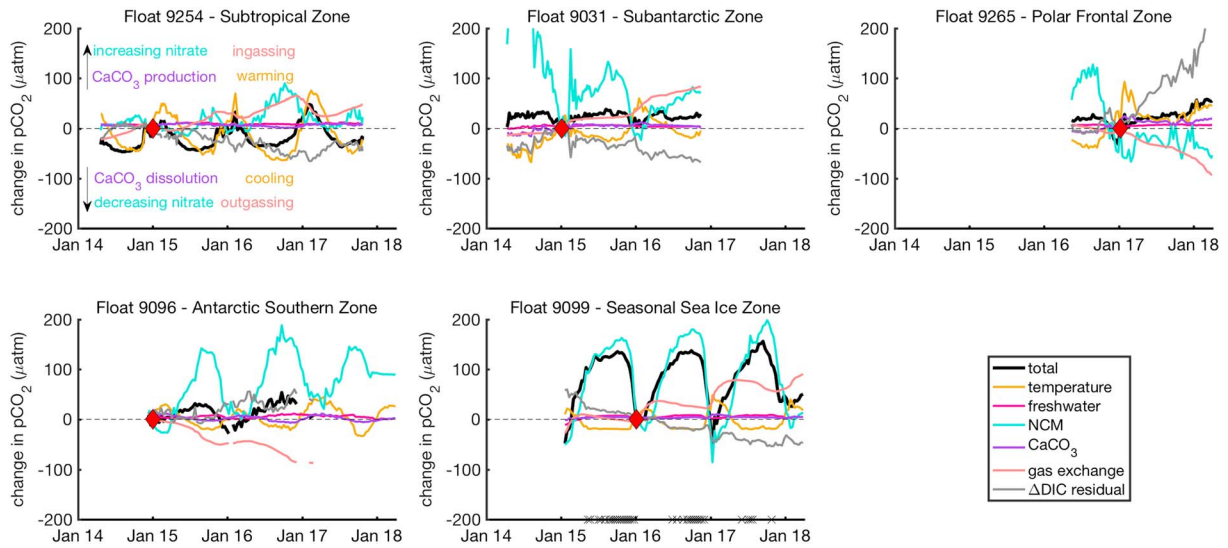
**Figure 5.** Decomposition of the drivers of pH and $\Omega_{Ar}$ from five representative floats. The red diamond in each subplot represents time zero, the black line represents cumulative observed changes relative to time zero, and the colored lines represent the cumulative contribution of each process to the cumulative observed changes relative to time zero. Black *crosses* along the *x* axis represent times when float 9099 sensed sea ice. NCM = net community metabolism; DIC = dissolved inorganic carbon.

The effect of $CO_2$ gas exchange with the atmosphere, $\Delta DIC_{gas}$, is also shown in Figure 4. Positive $\Delta DIC_{gas}$ indicates ingassing of $CO_2$. In the STZ, SAZ, and SSIZ the net effect of gas exchange is an increase in DIC over time of ~7–14 μmol/kg/yr. Because we do not observe a steady increase in DIC there must be a sink that is unaccounted for in our simple decomposition, as is represented by the $\Delta DIC_{residual}$ term. In the ASZ and the PFZ, gas exchange results in a net decrease in DIC over time. In the ASZ this decrease appears to be mostly compensated by the wintertime upwelling and entrainment of high DIC waters from below, being manifested as an increase in $\Delta DIC_{NCM}$ over the study period. In the PFZ, the increasing $\Delta DIC_{residual}$ term is compensated by both the decreasing $\Delta DIC_{gas}$ and $\Delta DIC_{NCM}$ terms, although it is difficult to say whether this is representative of an average year with such a short record. The $\Delta DIC_{residual}$ terms will be explored further in the discussion section 5.2.

### 4.3. Seasonal Drivers of pH and $\Omega_{Ar}$

Figure 5 shows the cumulative observed changes in pH and $\Omega_{Ar}$, as well as the contributions from the various drivers of DIC and TA shown in Figure 4. Because pH and $\Omega_{Ar}$ are directly affected by changes in T, we have added $\Delta pH_{temperature}$ and $\Delta \Omega_{temperature}$ terms to the decomposition. Across all zones the seasonal effects of changes in freshwater on pH and $\Omega_{Ar}$ are negligible and it is the competition between other terms that determine the observed seasonal cycle.

In spring and summer in all zones, surface warming causes an increase in $pCO_2$ resulting in a decrease in $\Delta pH_{temperature}$, and in fall and winter surface cooling reduces $pCO_2$ and increases $\Delta pH_{temperature}$. $\Delta pH_{temperature}$ is most pronounced in the STZ where seasonal swings in T are largest (Figure 3). Also in spring and summer, primary production removes DIC and increases $\Delta pH_{NCM}$, opposing the effects of T. In winter, increased respiration and upwelling of high DIC waters both lead to a decrease in $\Delta pH_{NCM}$. As the amplitude of the seasonal cycle in T decreases from the STZ southward to the SSIZ, $\Delta pH_{temperature}$ decreases. Similarly, as the seasonal cycle in $NO_3^-$ increases from the STZ southward to the SSIZ, $\Delta pH_{NCM}$ increases. This leads to a

**Figure 6.** Decomposition of the drivers of $pCO_2$ from five representative floats. The red diamond in each subplot represents time zero, the black line represents cumulative observed changes relative to time zero, and the colored lines represent the cumulative contribution of each process to the cumulative observed changes relative to time zero. Black *crosses* along the *x* axis represent times when float 9099 sensed sea ice. NCM = net community metabolism; DIC = dissolved inorganic carbon.

shift from a T-dominated system in the STZ to biologically dominated systems to the south. The SSIZ has the largest seasonal swing in pH with the SAZ, PFZ, and ASZ exhibiting relatively small seasonal cycles in pH. Because $CaCO_3$ production removes DIC and TA in a ratio of 1:2, it results in a net decrease in TA/DIC, an increase in $pCO_2$, and a decrease in pH. Dissolution of $CaCO_3$ or upwelling of deep waters has the opposite effect.

In contrast, $\Omega_{Ar}$ is less sensitive than pH to seasonal changes in T allowing NCM to determine the phasing and magnitude of the seasonal cycle in $\Omega_{Ar}$ in all five zones. In spring and summer, primary production removes DIC and increases $\Omega_{Ar}$. Respiration and wintertime upwelling and entrainment of high-DIC low-$\Omega_{Ar}$ water from below decrease $\Omega_{Ar}$ in the fall and winter. $CaCO_3$ production and dissolution plays only a minor role and tends to oppose the dominant NCM term.

Gas exchange results in net decreases in both pH and $\Omega_{Ar}$ in the STZ, SAZ, and SSIZ, and the opposite tendencies in the PFZ and ASZ. As with DIC, the $\Delta pH_{residual}$ and $\Delta\Omega_{residual}$ terms balance the gas fluxes except for in the ASZ where decreases in $\Delta pH_{NCM}$ and $\Delta\Omega_{NCM}$ over time balance the increase from gas exchange.

This seasonal decomposition illustrates that while the dominant seasonal drivers of pH vary across frontal regions, $\Omega_{Ar}$ is driven in all zones by a synergy of biological processes and wintertime upwelling and entrainment of high DIC water.

### 4.4. Seasonal Drivers of $pCO_2$

The observed changes in $pCO_2$ and the contributions from the various drivers relative to time zero are shown in Figure 6. These $\Delta pCO_2$ terms should not be confused with the traditional use of $\Delta pCO_2$, which is the difference in $pCO_2$ between the ocean and the atmosphere used to calculate air-sea $CO_2$ flux. As with pH and $\Omega_{Ar}$, $\Delta pCO_{2freshwater}$ and $\Delta pCO_{2CaCO3}$ both play a relatively small role ($<10\ \mu atm$) over the seasonal cycle. Because $pCO_2$ and $[H^+]$ covary, the drivers of $pCO_2$ are similar to those for pH. In all zones seasonal warming increases $pCO_2$, competing with NCM. This leads to higher $pCO_2$ in summer than in winter in the STZ where the seasonal cycle in T is largest and NCM is relatively weak. Moving southward the decreasing seasonal cycle in T and increasing NCM term results in lower $pCO_2$ in spring and summer than in fall and winter.

As with DIC, gas exchange would result in an increase in $pCO_2$ over time in the STZ, SAZ, and SSIZ and a decrease over time in the PFZ and the ASZ. However, as indicated by the decompositions, gas exchange is offset by various other terms in each sector. In the STZ, SAZ, and SSIZ the long-term increase in $pCO_2$ is
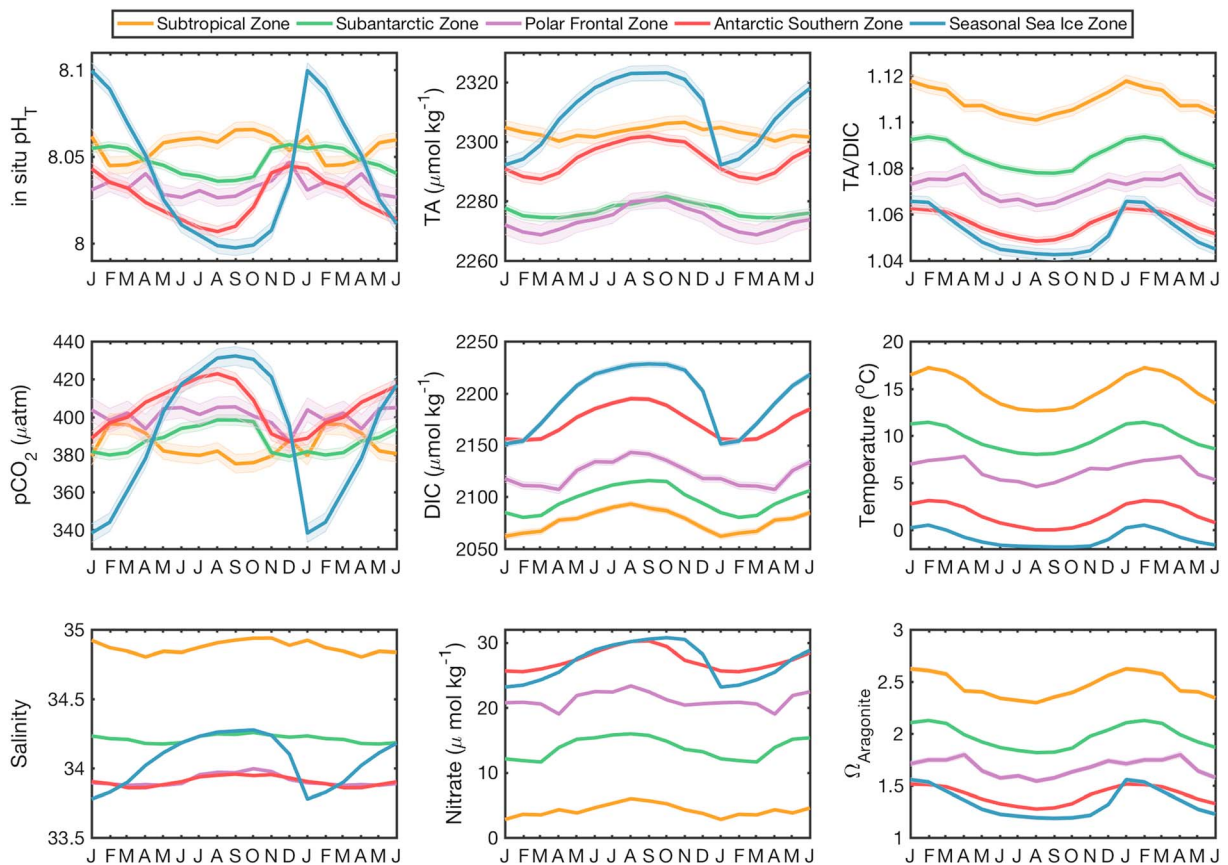
**Figure 7.** Monthly climatological surface seasonal cycles calculated using Locally Interpolated Alkalinity Regression total alkalinity (TA) values (Carter et al., 2018) with shading representing the standard error in the monthly mean. DIC = dissolved inorganic carbon.

balanced by the residual term, in the ASZ the decrease in $pCO_2$ is balanced by the NCM and residual terms, and in the PFZ the decrease in $pCO_2$ is balanced by the residual term. Again, the residual terms will be further explored in the discussion in section 5.2.

### 4.5. Climatological Seasonal Cycles

The float-based climatological surface ocean values for each of the five frontal regions are shown in Figure 7, and the mean values and amplitudes of the seasonal cycles in each parameter are summarized in Table 2. The amplitudes are calculated as the winter (June, July, or August) extreme monthly average value minus summer (December, January, or February) extreme monthly average value. The shading in Figure 7 represents the standard error of the monthly average. All monthly mean values and their standard deviations are provided in supporting information Table S1.

Climatological annual average TA is lowest in the SAZ and the PFZ where calcification removes TA from the surface ocean and transports it to the deep ocean, and highest in the STZ and SSIZ. The PFZ and ASZ have seasonal swings in TA of 12 ± 6 and 14 ± 4 μmol/kg, respectively, with higher TA in winter than in summer. This observed phasing in the PFZ conflicts with the T14 climatology for the corresponding region (Drake Area 1), which estimates summer TA to be higher than winter TA, but is consistent with the seasonal cycle in TA as observed from bottle data from the Drake Passage (D. Munro, personal communication, 17 December 2015). The seasonal cycle in TA is largest in the SSIZ (31 ± 4 μmol/kg) corresponding to the 0.50 seasonal swing in S and reinforced by the seasonal cycle in calcification. In the STZ the float data reveal only a 6 ± 5 μmol/kg average seasonal cycle in TA with the highest TA values in winter.

Climatological annual average DIC increases poleward from 2,079 ± 3 μmol/kg in the STZ to 2,202 ± 3 μmol/kg in the SSIZ, and TA/DIC and $\Omega_{Ar}$ both decrease poleward reflecting the decreased

**Table 2**
*Float-Based Climatological Values for the Surface and 200 m*

| | Surface | | 200 m |
|---|---|---|---|
| | Annual mean | Seasonal amplitude[a] | Annual mean |
| *Subtropical Zone* | | | |
| Temperature (°C) | 14.5 | −4.6 | 11.0 |
| Salinity | 34.88 | 0.13 | 34.83 |
| Nitrate (μmol/kg) | 4 | 3 | 11 |
| TA (μmol/kg) | 2,304 ± 2 | 6 ± 5 | 2,299 |
| DIC (μmol/kg) | 2,079 ± 3 | 31 ± 5 | 2,120 |
| $pCO_2$ (μatm) | 384 ± 5 | −21 ± 10 | 429 |
| In situ $pH_{Total}$ | 8.057 ± 0.004 | 0.021 ± 0.009 | 8.005 |
| $\Omega_{Aragonite}$ | 2.45 ± 0.02 | −0.33 ± 0.04 | 1.90 |
| $\Omega_{Calcite}$ | 3.81 ± 0.02 | −0.48 ± 0.04 | 2.98 |
| Mixed layer depth (m) | 86 | 135 | |
| *Subantarctic Zone* | | | |
| Temperature (°C) | 9.5 | −3.4 | 7.3 |
| Salinity | 34.22 | 0.08 | 34.34 |
| Nitrate (μmol/kg) | 14 | 4 | 19 |
| TA (μmol/kg)[b] | 2,278 ± 1 (2,275 ± 1) | 7 ± 3 (6 ± 2) | 2,280 |
| DIC (μmol/kg)[b] | 2,100 ± 2 (2,104 ± 1) | 35 ± 3 (28 ± 2) | 2,136 |
| $pCO_2$ (μatm)[b] | 388 ± 3 (390 ± 3) | 19 ± 5 (27 ± 6) | 442 |
| In situ $pH_{Total}$ | 8.047 ± 0.003 | −0.021 ± 0.005 | 7.987 |
| $\Omega_{Aragonite}$ | 1.95 ± 0.01 | −0.31 ± 0.02 | 1.58 |
| $\Omega_{Calcite}$ | 3.08 ± 0.01 | −0.47 ± 0.02 | 2.48 |
| Mixed layer depth (m) | 107 | 182 | |
| *Polar Frontal Zone* | | | |
| Temperature (°C) | 6.2 | −3.2 | 4.4 |
| Salinity | 33.92 | 0.12 | 34.09 |
| Nitrate (μmol/kg) | 21 | 4 | 26 |
| TA (μmol/kg)[b] | 2,275 ± 3 (2,268 ± 2) | 12 ± 6 (6 ± 5) | 2,278 |
| DIC (μmol/kg)[b] | 2,125 ± 3 (2,121 ± 3) | 36 ± 7 (29 ± 5) | 2,155 |
| $pCO_2$ (μatm)[b] | 400 ± 6 (396 ± 6) | 18 ± 12 (30 ± 12) | 446 |
| In situ $pH_{Total}$ | 8.033 ± 0.006 | −0.021 ± 0.011 | 7.980 |
| $\Omega_{Aragonite}$ | 1.66 ± 0.02 | −0.25 ± 0.04 | 1.38 |
| $\Omega_{Calcite}$ | 2.64 ± 0.03 | −0.39 ± 0.05 | 2.18 |
| Mixed layer depth (m) | 100 | 123 | |
| *Antarctic Southern Zone* | | | |
| Temperature (°C) | 1.4 | −3.1 | 1.4 |
| Salinity | 33.91 | 0.10 | 34.27 |
| Nitrate (μmol/kg) | 28 | 5 | 33 |
| TA (μmol/kg)[b] | 2,296 ± 2 (2,283 ± 1) | 14 ± 4 (10 ± 3) | 2,312 |
| DIC (μmol/kg)[b] | 2,176 ± 2 (2,163 ± 1) | 40 ± 4 (34 ± 3) | 2,225 |
| $pCO_2$ (μatm)[b] | 406 ± 3 (404 ± 4) | 36 ± 7 (36 ± 7) | 533 |
| In situ $pH_{Total}$ | 8.025 ± 0.003 | −0.038 ± 0.006 | 7.912 |
| $\Omega_{Aragonite}$ | 1.39 ± 0.01 | −0.24 ± 0.03 | 1.09 |
| $\Omega_{Calcite}$ | 2.22 ± 0.02 | −0.38 ± 0.03 | 1.72 |
| Mixed layer depth (m) | 95 | 84 | |
| *Seasonal Sea Ice Zone* | | | |
| Temperature (°C) | −1.1 | −2.3 | 0.4 |
| Salinity | 34.10 | 0.50 | 34.61 |
| Nitrate (μmol/kg) | 28 | 8 | 33 |
| TA (μmol/kg)[b] | 2,313 ± 3 (2,304 ± 2) | 31 ± 4 (38 ± 5) | 2,344 |
| DIC (μmol/kg)[b] | 2,202 ± 3 (2,193 ± 2) | 77 ± 5 (94 ± 5) | 2,262 |
| $pCO_2$ (μatm)[b] | 398 ± 5 (394 ± 4) | 94 ± 9 (116 ± 10) | 538 |
| In situ $pH_{Total}$ | 8.032 ± 0.005 | −0.102 ± 0.009 | 7.910 |
| $\Omega_{Aragonite}$ | 1.31 ± 0.02 | −0.37 ± 0.04 | 1.06 |
| $\Omega_{Calcite}$ | 2.09 ± 0.02 | −0.59 ± 0.04 | 1.67 |
| Mixed layer depth (m) | 86 | 95 | |

*Note.* TA = total alkalinity; DIC = dissolved inorganic carbon.
[a]Calculated as the winter minus summer extreme monthly mean values.   [b]Values outside (inside) parentheses are calculated using Locally Interpolated Alkalinity Regression (MLR) TA.
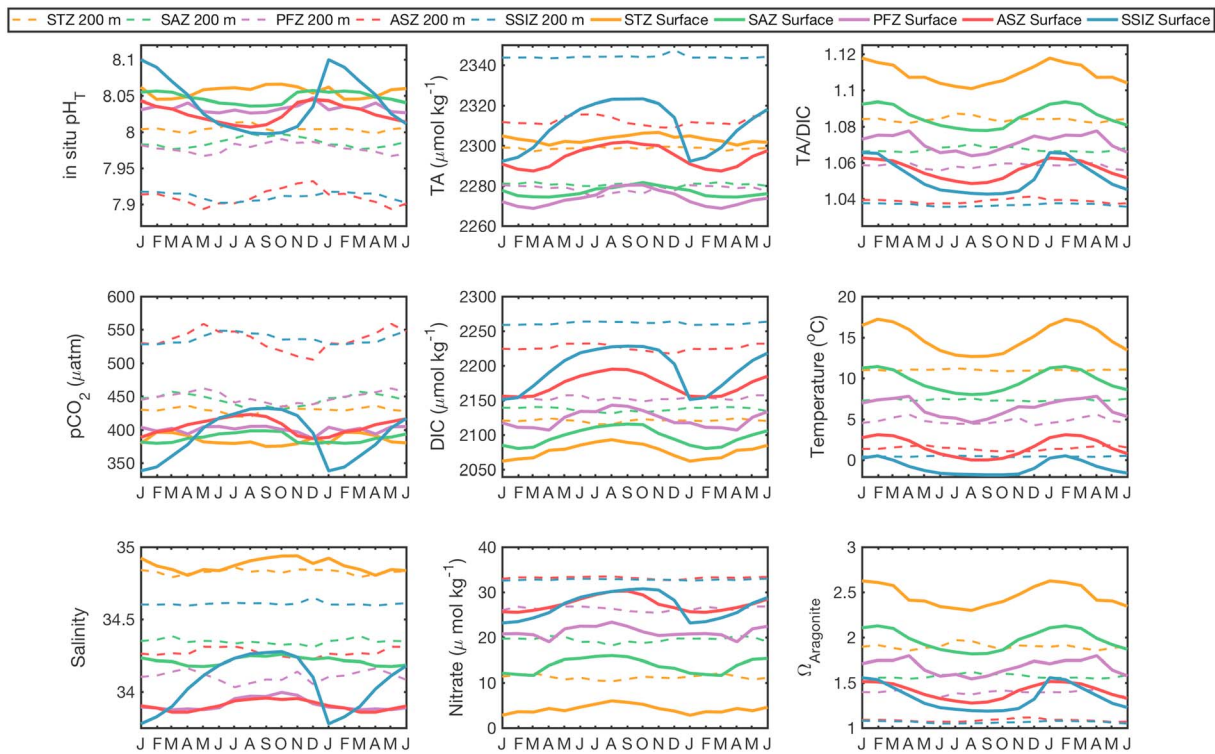
**Figure 8.** Monthly surface (solid lines) and 200 m (dashed lines) climatologies for the five frontal zones calculated using Locally Interpolated Alkalinity Regression total alkalinity (TA) values. DIC = dissolved inorganic carbon; STZ = Subtropical Zone; SAZ = Subantarctic Zone; PFZ = Polar Frontal Zone; ASZ = Antarctic Southern Zone; SSIZ = Seasonal Sea Ice Zone.

buffer capacity and increasingly corrosive conditions for calcifying organisms (Orr et al., 2005). The seasonal cycle in DIC is largest in the SSIZ ($77 \pm 5$ μmol/kg) and smallest in the STZ ($31 \pm 5$ μmol/kg). $NO_3^-$ also increases poleward from an annual average of 4 μmol/kg in the STZ to 28 μmol/kg in the ASZ and SSIZ. As with DIC, the seasonal cycle in $NO_3^-$ is largest in the SSIZ (7 μmol/kg) and in the ASZ (5 μmol/kg), with the ASZ leading the SSIZ springtime decrease (spring bloom) by 1–2 months on average.

Climatological annual mean surface pH generally decreases poleward from $8.057 \pm 0.004$ in the STZ to $8.025 \pm 0.003$ and $8.032 \pm 0.005$ in the ASZ and SSIZ, respectively, and $pCO_2$ generally increases poleward from $384 \pm 5$ μatm in the STZ to $406 \pm 3$ and $398 \pm 5$ μatm in the ASZ and SSIZ, respectively. The lowest monthly mean pH ($7.997 \pm 0.004$) is found in the SSIZ in September when upwelling of high DIC waters and respiration dominate, and when ice limits the amount of $CO_2$ that can escape to the atmosphere. The highest monthly average pH ($8.100 \pm 0.005$) is found in the SSIZ in January at the peak of the spring bloom. The SSIZ exhibits the largest climatological seasonal cycle in pH ($0.102 \pm 0.009$), where $pCO_2$ averages $432 \pm 4$ μatm in September, and $338 \pm 4$ μatm in January, a swing of $94 \pm 9$ μatm.

In the SSIZ, the seasonal amplitudes observed by any one float are often double the climatological average seasonal amplitude, and this underestimation results from the way that the climatology is created. A dampened climatological seasonal cycle results from differences in the timing of the extreme spring *ice-edge bloom* from float-to-float and because the floats may miss the peak of the bloom with sampling intervals of 10 days. Variety in the timing and magnitude of the spring ice-edge bloom is evident in the 34- and 33-μatm standard deviations in SSIZ climatological $pCO_2$ in January and February as compared to standard deviations in the other zones for those same months and the SSIZ in winter months (Table S1 and Figure S1). The observed ~150-μatm swing in $pCO_2$ for SSIZ float 9099 (Figure 3), with the lowest observed $pCO_2$ values persisting for less than 10 days, further supports the conclusion that the SSIZ climatological seasonal cycles are underestimated using our method. Underestimation is not a significant issue for the other zones as evidenced by the smaller variability in the monthly standard deviations (Table S1).
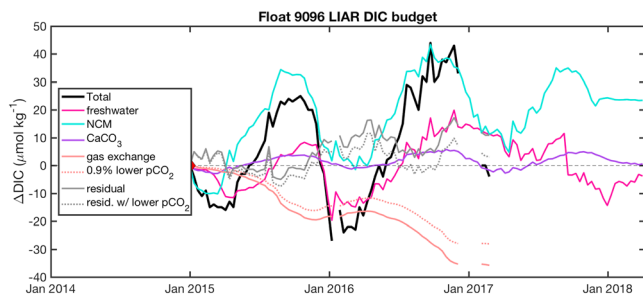
**Figure 9.** Illustration of the effect a systematic bias in the float-based $pCO_2$ estimate would have on the dissolved inorganic carbon (DIC) budget for float 9096 in the Antarctic Southern Zone. Dotted lines represent the results if *true* surface ocean $pCO_2$ were 0.9% lower than the float estimate. NCM = net community metabolism.

At 200 m, the climatological seasonal cycles for all parameters (Figure 8 and Table 2) are muted relative to the surface, whereas the north-south gradients are amplified and help explain the gradients we observe at the surface between the zones. At 200 m, DIC, $pCO_2$, and $NO_3^-$ increase poleward and pH, $\Omega_{Ar}$, and TA/DIC decrease poleward reflecting the increased influence of old upwelled nutrient- and carbon-rich deep waters in the southernmost zones. In the SAZ, PFZ, and ASZ where wintertime mixed layers can reach 200 m or more a seasonal cycle is distinguishable at 200 m in most parameters.

## 5. Discussion

### 5.1. Assumptions and Uncertainties

There are several assumptions and uncertainties inherent in this analysis. First, we are assuming that floats are representative of the larger Southern Ocean zones to which we assign them. In reality, floats move mostly along with the prevailing currents at a depth of 1,000 m and it is possible that a sampling bias occurs as a result of where the floats were deployed or if they tend to congregate near or avoid certain oceanographic features. For example, SOCCOM float data are currently weighted toward the Pacific sector, with the Atlantic and Indian sectors not as well sampled due to limitations in available deployment cruises, and we know that there are gradients in carbonate system parameters and nutrients between the three basins (Garcia et al., 2013; Key et al., 2015).

Second, by using only 4 years of SOCCOM float data, we are not able to assess decadal-scale variability in seasonality, an important time scale for Southern Ocean carbon fluxes (DeVries et al., 2017; Landschützer et al., 2014; Le Quéré et al., 2007; McKinley et al., 2017). Over the years 2014–2017 the Southern Annular Mode has been in a positive phase (Marshall, 2003), which causes anomalously high surface ocean $pCO_2$ driven mostly by anomalous upwelling of high DIC waters in the ASZ, PFZ, and SAZ and subsequent increased outgassing of natural $CO_2$ (Lovenduski et al., 2007).

Third, because the floats are only directly measuring pH and the remainder of the carbonate system must be estimated, it is necessary to consider how uncertainties in the estimated parameters could affect the results. As noted in the methods, the uncertainties in pH and TA are 0.01 and 5 μmol/kg, respectively, leading to uncertainties in DIC, $pCO_2$, $\Omega_{Ar}$, and $\Omega_{Ca}$ of 4 μmol/kg, 2.7% (11 μatm at a $pCO_2$ of 400 μatm; Williams et al., 2017), 0.04, and 0.05, respectively. For the calculation of climatological seasonal cycles, any component of the uncertainties that is random will average out to be insignificant with a large sample number. However, any systematic bias would result in a systematic bias in the climatological values, which is particularly important for $pCO_2$, as it is the gradient between the ocean and atmosphere, which determines the air-sea *F*. Williams et al. (2017) carefully considered all potential sources of bias and found that while the systematic uncertainty in float-estimated $pCO_2$ could be as much as 1.8% (7.2 μatm at a $pCO_2$ of 400 μatm), a comparison between initial float profiles and shipboard measurements of $pCO_2$ indicated that float-estimated $pCO_2$ values were biased high by only 3.7 μatm (0.9% of 400 μatm). Figure 9 illustrates how a systematic bias of this magnitude would affect the DIC budget results for float 9096 in the ASZ, which has a net outgassing of $CO_2$. This figure compares $\Delta DIC_{gas}$ with $\Delta DIC_{gas}$ if true surface ocean $pCO_2$ were 0.9% lower than the float-based estimate. The net effect of this potential bias in float-based $pCO_2$ is 20% less outgassing of $CO_2$ but no change in the direction of gas exchange. The $\Delta DIC_{freshwater}$, $\Delta DIC_{NCM}$, and $\Delta DIC_{CaCO3}$ terms are unaffected by this bias but, because $\Delta DIC_{residual}$ is calculated by difference between observed $\Delta DIC$ and the sum of the other $\Delta DIC$ terms, $\Delta DIC_{residual}$ would be affected by any systematic bias in $pCO_2$.

In terms of the surface $NO_3^-$, TA, and DIC budgets, we have made some simplifications and these choices could also affect the budget results. For example, the NCM terms in each budget are based on the assumption that the $\Delta NO_{3residual}^-$ term is zero, meaning that changes in $NO_3^-$ not accounted for by $\Delta NO_{3freshwater}^-$ represent primary production or respiration occurring either in situ or elsewhere in the past and affect DIC at a ratio of $\Delta NO_3^- : \Delta DIC = 16:117$ (Sarmiento & Gruber, 2006). This would not hold true if, in reality, this ratio is seasonally or spatially variant (Arrigo, 2005), or if the ratios of $NO_3^-$:DIC of waters brought into the surface mixed layer either horizontally or vertically are different from the theoretical value. In the STZ, for example,

the surface $NO_3^-$ is 2–6 $\mu$mol/kg and the submixed layer (MLD + 25 m) nitrate is 10–12 $\mu$mol/kg resulting in a vertical change of up to 10 $\mu$mol/kg. Observed vertical changes in DIC over the same depth range in this region are only 41 $\mu$mol/kg, not the expected change of 73 $\mu$mol/kg (10 $\mu$mol/kg $NO_3^-$ $\times$ 117/16). As a result, $\Delta DIC_{NCM}$ calculated from $\Delta NO_{3NCM}^-$ during times when there is entrainment or mixing with water from below the mixed layer would tend be an ~50% overestimate in the STZ. This overestimation in $\Delta DIC_{NCM}$ would only serve to increase the magnitude of the missing DIC sink represented by the $\Delta DIC_{residual}$ term in the STZ and does not change our overall results. South of the STZ this assumption is less of an issue because the vertical gradients in $NO_3^-$ and DIC follow the assumed ratio more closely.

## 5.2. Closing the Carbon Budget

Several of the floats have relatively large residual terms in their decompositions of DIC from section 4.2. In the STZ, SAZ, and SSIZ, net ingassing of $CO_2$ from the atmosphere necessitates a residual sink for DIC and $pCO_2$ (Figures 4 and 6).

In the STZ, this *missing sink* for DIC could be explained by the geostrophic divergence of DIC in the vicinity of float 9254, which is located east of the North Island of New Zealand. This region experiences southward flow as part of the western edge of the subtropical gyre where low DIC, low nutrient waters are transported into the region from the north. Winter mixing then brings nutrients from below into the mixed layer, fueling primary production that drives ingassing of $CO_2$ and increases DIC and $pCO_2$. This extra DIC is subsequently transported to the south. This mechanism was suggested by Ayers and Lozier (2012) in the western North Pacific, who found geostrophic advection could account for a 113 $\pm$ 8 $\mu$atm/year decrease in $pCO_2$. For float 9254 the residual term is closer to ~30 $\mu$atm/year (Figure 6) but as discussed in section 5.1 this might be an underestimate because the calculations were based on the assumption of constant stoichiometry. In the SAZ where the surface flow is predominantly to the north and driven by Ekman transport, there should be a buildup of DIC due to convergence of surface water from Ekman transport. In order for the $\Delta DIC_{residual}$ term to be negative there must be an even larger sink of DIC to the north. This could be accounted for by the subduction of DIC into subantarctic mode and Antarctic intermediate waters (Ito et al., 2010). In the SSIZ both the northward transport of high DIC waters and export of organic matter to the deep ocean (peaking in spring) could help account for the residual sink for DIC.

In the PFZ and ASZ we estimate a decrease in DIC from outgassing of $CO_2$ of 15–20 $\mu$mol/kg/yr that must be balanced. In the ASZ this outgassing appears to be mostly balanced by a net increase in the $\Delta DIC_{NCM}$ term likely representing winter entrainment and mixing with high DIC waters below. In the PFZ the outgassing is balanced by the $\Delta DIC_{residual}$ term, which could again be explained by an Ekman convergence of surface water where higher DIC waters are being transported into the region from the ASZ to the south.

Our results from float-based carbon budgets reinforce the finding of Ayers and Lozier (2012) that it is both local biological processes and the surface gradients in DIC which determine the dominant locations of net uptake of $CO_2$. In contrast, the regions of net outgassing of $CO_2$ are determined by coincidence of upwelling of high-DIC waters and Ekman convergence of DIC as is found in the PFZ and ASZ. The SSIZ would also likely be a weaker net sink for $CO_2$ were it not for the wintertime ice cover that limits outgassing. If Southern Ocean sea ice cover begins to decline as has been predicted (Intergovernmental Panel on Climate Change, 2013) it could result in a shift toward more wintertime outgassing of $CO_2$, reducing the magnitude of the Southern Ocean $CO_2$ sink.

## 5.3. Comparison With Existing Data Sets and Climatologies

In light of the new winter data supplied by SOCCOM floats, it is useful to evaluate these float-based climatological seasonal cycles against existing climatological products. Comparisons of the surface monthly mean values, seasonal amplitudes, and drivers are made with values reported in T14. The T14 climatology of carbonate system parameters was derived from a monthly climatology for $pCO_2$ (Takahashi et al., 2009) created from underway $pCO_2$ measurements. This $pCO_2$ climatology was combined with an estimate for TA based on regional empirical potential alkalinity (PALK = TA + $NO_3^-$) versus S relationships. The PALK-based estimate for TA was combined with climatological $pCO_2$ to calculate monthly climatological surface ocean DIC, pH, $\Omega_{Ar}$, and $\Omega_{Ca}$ globally in 4° $\times$ 5° grid boxes for the reference year 2005. The uncertainties in T14 $pCO_2$, TA, DIC, pH, and $\Omega_{Ar}$ are $\pm$10 $\mu$atm, $\pm$10 $\mu$mol/kg, $\pm$10 $\mu$mol/kg, $\pm$0.01, and $\pm$ 0.06, respectively. For comparison
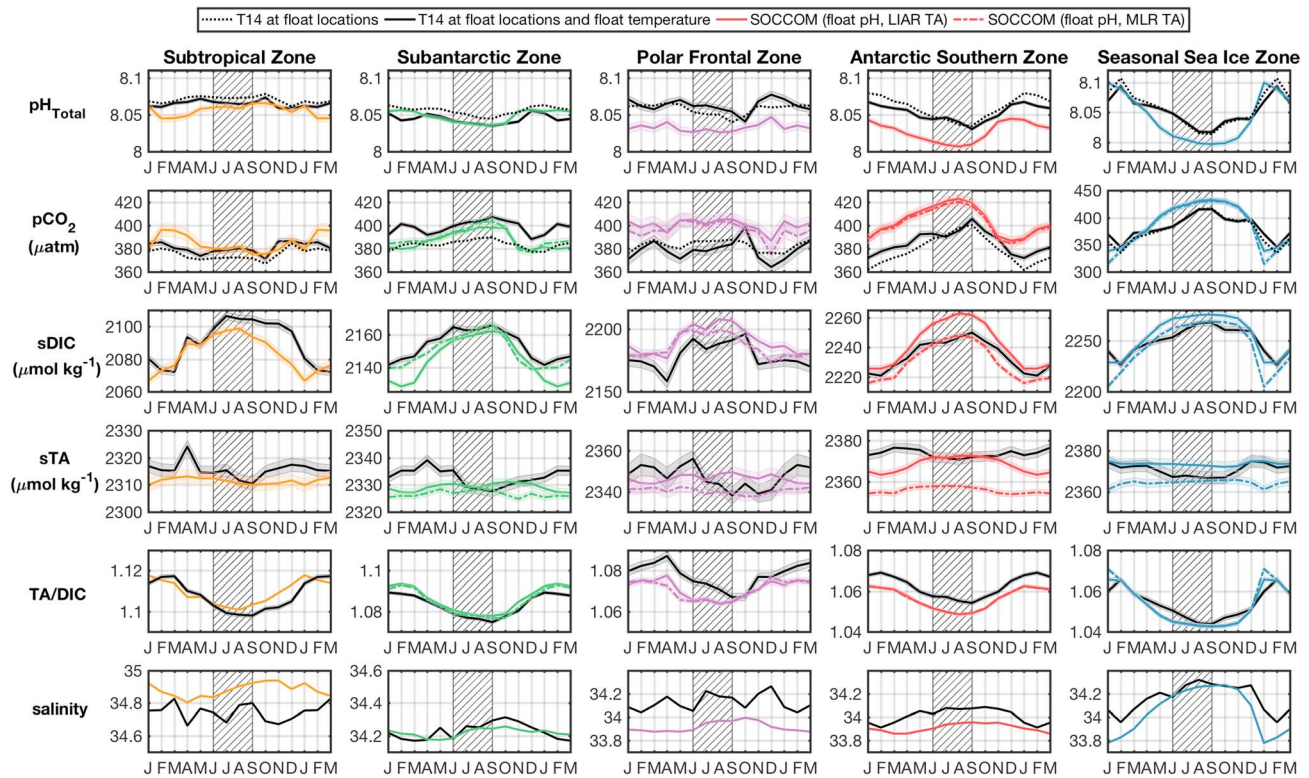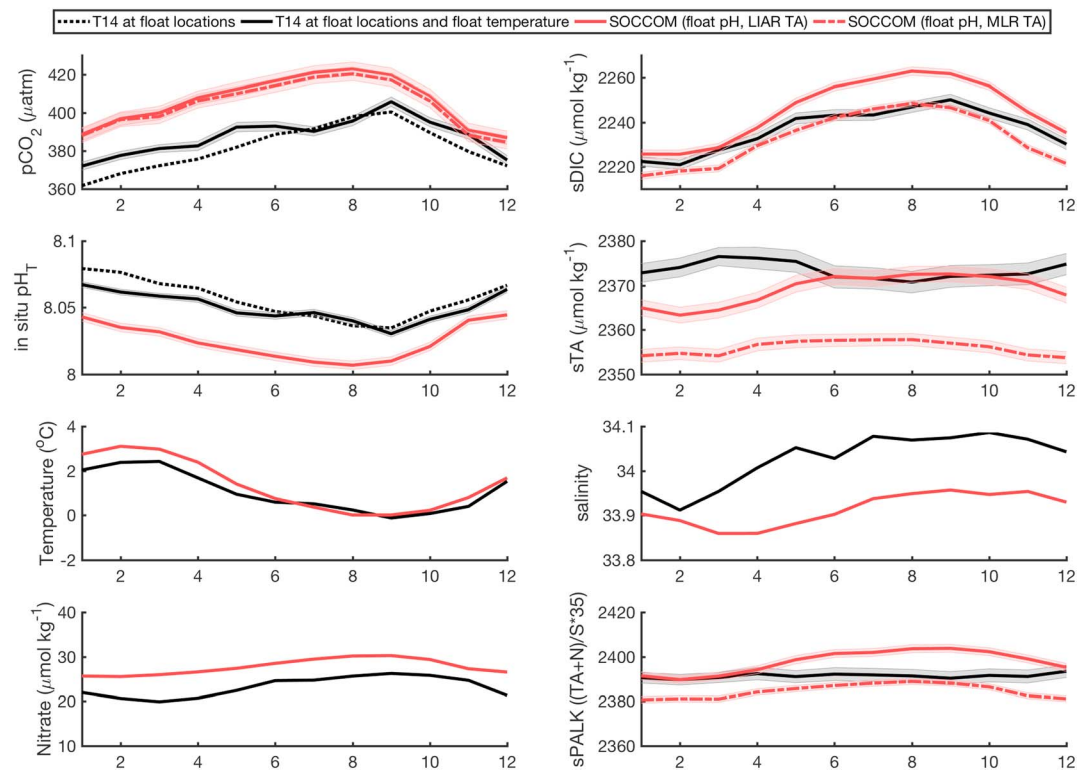
**Figure 10.** Southern Ocean Carbon and Climate Observations and Modeling (SOCCOM) float-based climatological seasonal cycles in pH, $pCO_2$, sDIC, sTA, TA/DIC, and S calculated using Locally Interpolated Alkalinity Regression (LIAR) total alkalinity (TA; solid colored lines, Carter et al., 2018) and MLR TA (dot-dashed colored lines, Williams et al., 2017) with shading representing the standard error in the monthly mean. Takahashi et al. (2014) climatological seasonal cycles from the month and location of each float are adjusted for anthropogenic change and recalculated at float-observed temperatures (black solid lines) with shading representing the standard error in the monthly mean. The hatched area in each subplot represents Austral winter.

with the SOCCOM floats, the T14 climatological data are first subsampled at the location and time of year of each float profile. The T14 climatological data are then adjusted from the climatological reference year (2005) to the float profile year (ranging between 2014 and 2017) according to the reported rates of anthropogenic change in T14 Table 2. Specifically, the STZ data were adjusted according to the T14 ESTOC rates, the SAZ and PFZ according to T14 Drake Area 1 rates, and the ASZ and SSIZ according to T14 Drake Area 4 rates. To make the comparison more direct for the strongly T-dependent variables pH and $pCO_2$, the T14 climatological values were recalculated at the float T using CO2SYS (van Heuven et al., 2011). Monthly T14 climatologies for each zone were created following the same averaging procedure as described in section 3. The results are shown in Figure 10 and documented in Table S2. Table S3 reports the difference between the SOCCOM climatological values and the T14 values at the float locations and float temperatures.

The differences between climatological monthly values for SOCCOM floats and T14 in situ $pH_{Total}$, $pCO_2$, salinity-normalized DIC (sDIC = DIC/ S · 35), salinity-normalized TA (sTA = TA/S · 35), TA/DIC, and S are shown in Figure 10. Climatologies based on both LIAR and MLR TA are shown, with shading representing the uncertainty in the monthly mean. In both the STZ and the SAZ the climatological values from T14 for all carbonate system parameters match the floats relatively well after adjusting for T differences. However, in the PFZ, ASZ, and SSIZ, the T14 climatology underestimates $pCO_2$ and overestimates pH throughout most of the year even after adjusting for T differences and anthropogenic change, with the largest discrepanices in Austral winter months (hatched areas). These significant differences in $pCO_2$ have been previously documented and are not surprising given that there were very few wintertime observations outside of Drake Passage prior to SOCCOM (Williams et al., 2017). This discrepancy in $pCO_2$ of up to 34 µatm during wintertime could be caused by a significant change in Southern Ocean circulation between the T14 climatological data set (reference year 2005) and 2014–2017 where a positive phasing in the Southern Annular Mode has resulted in anomalously large volumes of upwelled high-DIC waters (Lovenduski et al., 2007). Conversely, differences could be methodological.

**Figure 11.** Climatological values for the Antarctic Southern Zone as observed from Southern Ocean Carbon and Climate Observations and Modeling (SOCCOM) floats (Locally Interpolated Alkalinity Regression (LIAR) total alkalinity (TA) in solid red lines, MLR TA in dashed red lines), T14 climatology adjusted for anthropogenic change (black dashed lines), and T14 climatology adjusted for anthropogenic change and observed temperature differences (black solid lines) with shading representing the standard error in the monthly mean.

An increase of 30 µatm in $pCO_2$ requires only a 10 µmol/kg increase in DIC. We do observe significant increases in both LIAR- and MLR-based sDIC between T14 and SOCCOM in the PFZ, ASZ, and SSIZ, with the exception of in the ASZ where the SOCCOM MLR sDIC is similar to T14. In the T14 climatological data set, only $pCO_2$ is directly measured and in the SOCCOM data set only pH is directly measured, and in both data sets the directly measured parameter is combined with an estimate for TA to calculate the other carbonate system variables. When calculating pH from $pCO_2$, or vice versa, the result depends mostly on the measured variable and less so on the TA estimate (Dickson & Riley, 1978; Williams et al., 2017). However, calculating accurate DIC from pH or $pCO_2$ depends more heavily on the accuracy of the TA estimate. It therefore follows that any bias in estimated TA between the two data sets would result in a bias in DIC but not in pH or $pCO_2$. The T14 TA estimate is derived from an empirical relationship of PALK (TA + $NO_3^-$) as a function of S, and the SOCCOM TA is estimated using independent empirical methods relying on float-measured T, S, P, $O_2$, and location.

To further examine the differences between the two data sets, we take a closer look at the SOCCOM/T14 comparison in the ASZ (Figure 11). The salinity-normalized PALK values for T14 fall within the SOCCOM estimates, suggesting that the PALK versus S relationships used to create the T14 TA climatologies hold for 2014–2017. However, the T14 sTA is higher than both SOCCOM TA products, on average, and higher than the MLR TA product by up to 20 µmol/kg. This positive bias in T14 sTA can be partially explained by the ~4 µmol/kg increase in $NO_3^-$ between the two data sets (Figure 11), which would cause the T14 sTA (derived from PALK) to be 4 µmol/kg higher than SOCCOM sTA year round. Because biases in TA propagate through the calculations almost directly as biases in DIC, direct comparisons of DIC are difficult.

One quantity that can be more easily compared is the TA/DIC (Figure 10). In the PFZ and ASZ, the SOCCOM TA/DIC is lower than T14 by around 0.005 on top of the 0.004 per decade increase expected from anthropogenic change. This additional increase in surface TA/DIC could be explained by increased influence of lower

TA/DIC waters from below the mixed layer. These low TA/DIC waters are present at 200 m or shallower south of the subantarctic front (Figures 1 and 8) and deep winter mixing reaches these depths. Also, $NO_3^-$ concentrations in the ASZ and PFZ are 4 and 6 $\mu$mol/kg higher than T14 year round (Figure 11 and supporting information Figure S4 and Table S3) suggesting increased influence of deeper waters at the surface. Similarly, south of the PF along the meridional SR03 line south of Australia Pardo et al. (2017) found an increase in silicate in surface waters of 0.36 ± 0.06 $\mu$mol/kg/yr. Using a silicate to $NO_3^-$ ratio of 1.05 (Brzezinski, 2004) this silicate increase corresponds to a 3.7 ± 0.6 $\mu$mol/kg increase in $NO_3^-$ between 2005 and our study period, matching well with our observations. Pardo et al. (2017) also found a 3 times faster shoaling in the aragonite saturation horizon south of the Polar Front than to the north, indicating an increase in upwelling and meridional overturning south of the ACC.

## 6. Conclusions

In this study we have decomposed the drivers of the carbonate system over several annual cycles in each of five Southern Ocean frontal zones and created climatological seasonal cycles for the surface and for 200 m in each zone. By analyzing each frontal zone separately, we have illustrated the diversity of regimes ranging from a temperature-dominated system in the subtropics to a biological- and sea-ice-dominated system closer to the Antarctic Continent. We find that net ingassing in the STZ, SAZ, and SSIZ and net outgassing in the ASZ and PFZ cannot be accounted for by biological processes alone and that the interplay between surface gradients in carbon, physical transport, and biological processes is important for determining the source/sink status of each zone. At this time there are not enough floats to analyze the Pacific, Atlantic, and Indian sectors separately but the distribution of floats is on track to improve and this topic is ripe for future work.

Comparisons with the Takahashi et al. (2014) climatology show good agreement north of the ACC and worse agreement to the south, especially in winter months, with SOCCOM observing elevated $pCO_2$ and decreased pH relative to the climatology. South of the ACC the annual mean pH is lower than Takahashi et al. (2014) by between 0.02 and 0.03 and annual mean $pCO_2$ is higher by 11 to 21 $\mu$atm. The phasing and amplitudes of the seasonal cycles are not significantly different from Takahashi et al. (2014) except for TA in the STZ, SAZ, and PFZ where SOCCOM floats observe the opposite phasing from Takahashi et al. (2014). Also, the SOCCOM floats observe a larger seasonal cycle than Takahashi et al. (2014) in nearly all parameters in the SSIZ. These discrepancies are likely due, in part, to a lack of wintertime observations in most of the Southern Ocean before SOCCOM and may also be due to large-scale increases in upwelling and entrainment of older carbon- and nutrient-rich deep waters into the region associated with the ongoing positive phase of the Southern Annular Mode. Observed increases in surface nitrate and decreases in surface TA/DIC relative to Takahashi et al. (2014), which exceed the expected anthropogenic change over the period 2005–2016, reinforce the hypothesis that SOCCOM is observing a large-scale shift in Southern Ocean circulation relative to the early 2000s.

The results of this study demonstrate how biogeochemical profiling floats are improving our understanding of the current state of the carbonate system in the Southern Ocean, and how they can improve baseline observations needed to validate model behavior. These new observations can also decrease uncertainties in the global carbon budget by providing persistent observations of the carbonate system over a wide range of spatial and temporal scales that shipboard surveys alone cannot offer. By measuring carbon and nutrients together, these floats provide a unique opportunity to create biogeochemical budgets, which can improve our understanding of the ocean carbon cycle. With continued deployment of biogeochemical profiling floats we can use them as a tool to continue to develop our understanding of the Southern Ocean's role in climate on longer time scales and its relationship with natural modes of variability as well as human-induced change.

## References

Arrigo, K. R. (2005). Marine microorganisms and global nutrient cycles. *Nature*, *437*(7057), 349–355. https://doi.org/10.1038/nature04159

Ayers, J. M., & Lozier, M. S. (2012). Unraveling dynamical controls on the North Pacific carbon sink. *Journal of Geophysical Research*, *117*, C01017. https://doi.org/10.1029/2011JC007368

Brzezinski, M. A. (2004). The Si:C:N ratio of marine diatoms: Interpsecific variability and the effect of some environmental variables. *Journal of Phycology*, *21*(3), 347–357. https://doi.org/10.1111/j.0022-3646.1985.00347.x

Carter, B. R., Feely, R. A., Williams, N. L., Dickson, A. G., Fong, M. B., & Takeshita, Y. (2018). Updated methods for global locally interpolated estimation of alkalinity, pH, and nitrate. *Limnology and Oceanography: Methods*, *16*(2), 119–131. https://doi.org/10.1002/lom3.10232

DeVries, T., Holzer, M., & Primeau, F. (2017). Recent increase in oceanic carbon uptake driven by weaker upper-ocean overturning. *Nature*, *542*(7640), 215–218. https://doi.org/10.1038/nature21068

Dickson, A. G. (1990). Standard potential of the reaction: AgCl (s) + 1/2 H2(g) = Ag (s) + HCl (aq), and the standard acidity constant of the ion $HSO_4^-$ in synthetic sea water from 273.15 to 318.15 K. *The Journal of Chemical Thermodynamics*, *22*(2), 113–127. https://doi.org/10.1016/0021-9614(90)90074-Z

Dickson, A. G., & Riley, J. P. (1978). The effect of analytical error on the evaluation of the components of the aquatic carbon-dioxide system. *Marine Chemistry*, *6*(1), 77–85. https://doi.org/10.1016/0304-4203(78)90008-7

Dickson, A. G., Sabine, C. L., & Christian, J. R. (2007). Guide to best practices for ocean CO2 measurements, PICES Special Publication 3. https://doi.org/10.1039/9781847550835.

Dong, S., Sprintall, J., Gille, S. T., & Talley, L. (2008). Southern Ocean mixed-layer depth from Argo float profiles. *Journal of Geophysical Research*, *113*, C06013. https://doi.org/10.1029/2006JC004051

Frölicher, T. L., Sarmiento, J. L., Paynter, D. J., Dunne, J. P., Krasting, J. P., & Winton, M. (2015). Dominance of the Southern Ocean in anthropogenic carbon and heat uptake in CMIP5 models. *Journal of Climate*, *28*(2), 862–886. https://doi.org/10.1175/JCLI-D-14-00117.1

Garcia, H. E., Locarnini, R. A., Boyer, T. P., Antonov, J. I., Baranova, O. K., Zweng, M. M., et al. (2013). *World Ocean Atlas 2013, Volume 4: Dissolved Inorganic Nutrients (phosphate, nitrate, silicate)*. In S. Levitus & A. Mishonov (Eds.) (76th ed.). Silver Spring, MD.

Intergovernmental Panel on Climate Change (2013). *Climate Change 2013: The Physical Science Basis. Contribution of Working Group I to the Fifth Assessment Report of the Intergovernmental Panel on Climate Change*, T. F. Stocker et al. (Eds.). Cambridge University Press, Cambridge, UK, and New York.

Ito, T., Woloszyn, M., & Mazloff, M. (2010). Anthropogenic carbon dioxide transport in the Southern Ocean driven by Ekman flow. *Nature*, *463*(7277), 80–83. https://doi.org/10.1038/nature08687

Johnson, K. S., Jannasch, H. W., Coletti, L. J., Elrod, V. A., Martz, T. R., Takeshita, Y., et al. (2016). Deep-Sea DuraFET: A pressure tolerant pH sensor designed for global sensor networks. *Analytical Chemistry*, *88*(6), 3249–3256. https://doi.org/10.1021/acs.analchem.5b04653

Johnson, K. S., Plant, J. N., Coletti, L. J., Jannasch, H. W., Sakamoto, C. M., Riser, S. C., et al. (2017). Biogeochemical sensor performance in the SOCCOM profiling float array. *Journal of Geophysical Research: Oceans*, *122*, 6416–6436. https://doi.org/10.1002/2017JC012838

Jones, E. M., Fenton, M., Meredith, M. P., Clargo, N. M., Ossebaar, S., Ducklow, H. W., et al. (2017). Ocean acidification and calcium carbonate saturation states in the coastal zone of the West Antarctic Peninsula. *Deep-Sea Research Part II: Topical Studies in Oceanography*, *139*, 181–194. https://doi.org/10.1016/j.dsr2.2017.01.007

Kalnay, E., Kanamitsu, M., Kistler, R., Collins, W., Deaven, D., Gandin, L., et al. (1996). The NCEP/NCAR 40-year reanalysis project. *Bulletin of the American Meteorological Society*, *77*(3), 437–471. https://doi.org/10.1175/1520-0477(1996)077%3C0437:TNYRP%3E2.0.CO;2

Key, R. M., Olsen, A., van Heuven, S., Lauvset, S. K., Velo, A., Lin, X., et al. (2015). Global Ocean Data Analysis Project, Version 2 (GLODAPv2), ORNL/CDIAC-162, NDP-093. Oak Ridge, Tennessee: Carbon Dioxide Information Analysis Center, Oak Ridge National Laboratory, US Dept. of Energy. https://doi.org/10.3334/CDIAC/OTG.NDP093_GLODAPv2

Landschützer, P., Gruber, N., Bakker, D. C. E., & Schuster, U. (2014). Recent variability of the global ocean carbon sink. *Global Biogeochemical Cycles*, *28*, 927–949. https://doi.org/10.1002/2014GB004853

Landschützer, P., Gruber, N., Bakker, D. C. E., Schuster, U., Nakaoka, S., Payne, M. R., et al. (2013). A neural network-based estimate of the seasonal to inter-annual variability of the Atlantic Ocean carbon sink. *Biogeosciences*, *10*(11), 7793–7815. https://doi.org/10.5194/bg-10-7793-2013

Law, C. S., Rickard, G. J., Mikaloff-Fletcher, S. E., Pinkerton, M. H., Behrens, E., Chiswell, S. M., & Currie, K. (2017). Climate change projections for the surface ocean around New Zealand. *New Zealand Journal of Marine and Freshwater Research*, *8330*, 1–27. https://doi.org/10.1080/00288330.2017.1390772

Le Quéré, C., Andrew, R. M., Canadell, J. G., Sitch, S., Korsbakken, J. I., Peters, G. P., et al. (2016). Global carbon budget 2016. *Earth System Science Data*, *8*(2), 605–649. https://doi.org/10.5194/essd-8-605-2016

Le Quéré, C., Rödenbeck, C., Buitenhuis, E. T., Conway, T. J., Langenfelds, R., Gomez, A., et al. (2007). Saturation of the southern ocean CO2 sink due to recent climate change. *Science*, *316*(5832), 1735–1738. https://doi.org/10.1126/science.1136188

Lee, K., Kim, T.-W., Byrne, R. H., Millero, F. J., Feely, R. A., & Liu, Y.-M. (2010). The universal ratio of boron to chlorinity for the North Pacific and North Atlantic oceans. *Geochimica et Cosmochimica Acta*, *74*(6), 1801–1811. https://doi.org/10.1016/j.gca.2009.12.027

Lovenduski, N. S., Gruber, N., Doney, S. C., & Lima, I. D. (2007). Enhanced CO2 outgassing in the Southern Ocean from a positive phase of the Southern Annular Mode. *Global Biogeochemical Cycles*, *21*, GB2026. https://doi.org/10.1029/2006GB002900

Lueker, T. J., Dickson, A. G., & Keeling, C. D. (2000). Ocean pCO2 calculated from dissolved inorganic carbon, alkalinity, and equations for $K_1$ and $K_2$: Validation based on laboratory measurements of CO2 in gas and seawater at equilibrium. *Marine Chemistry*, *70*(1–3), 105–119. https://doi.org/10.1016/S0304-4203(00)00022-0

Marshall, G. J. (2003). Trend in the southern annular mode from observations and reanalyses. *Journal of Climate*, *16*(24), 4134–4143. https://doi.org/10.1175/1520-0442(2003)016%3C4134:TITSAM%3E2.0.CO;2

McKinley, G. A., Fay, A. R., Lovenduski, N. S., & Pilcher, D. J. (2017). Natural variability and anthropogenic trends in the ocean carbon sink. *Annual Review of Marine Science*, *9*(1), 125–150. https://doi.org/10.1146/annurev-marine-010816-060529

McNeil, B. I., Sweeney, C., & Gibson, J. A. E. (2011). Short note: Natural seasonal variability of aragonite saturation state within two Antarctic coastal ocean sites. *Antarctic Science*, *23*(4), 411–412. https://doi.org/10.1017/S0954102011000204

Munro, D. R., Lovenduski, N. S., Stephens, B. B., Newberger, T., Arrigo, K. R., Takahashi, T., et al. (2015). Estimates of net community production in the Southern Ocean determined from time series observations (2002–2011) of nutrients, dissolved inorganic carbon, and surface ocean pCO2 in Drake Passage. *Deep-Sea Research Part II: Topical Studies in Oceanography*, *114*, 49–63. https://doi.org/10.1016/j.dsr2.2014.12.014

Orr, J. C., Epitalon, J.-M., & Gattuso, J.-P. (2015). Comparison of ten packages that compute ocean carbonate chemistry. *Biogeosciences*, *12*(5), 1483–1510. https://doi.org/10.5194/bg-12-1483-2015

Orr, J. C., Fabry, V. J., Aumont, O., Bopp, L., Doney, S. C., Feely, R. A., et al. (2005). Anthropogenic ocean acidification over the twenty-first century and its impact on calcifying organisms. *Nature*, *437*(7059), 681–686. https://doi.org/10.1038/nature04095

Orsi, A. H., Whitworth, T. I., & Nowlin, W. D. J. (1995). On the meridional extent and fronts of the Antarctic Circumpolar Current. *Deep Sea Research Part I: Oceanographic Research Papers*, *42*(5), 641–673. https://doi.org/10.1016/0967-0637(95)00021-W

Pardo, P. C., Tilbrook, B., Langlais, C., Trull, T. W., & Rintoul, S. R. (2017). Carbon uptake and biogeochemical change in the Southern Ocean, south of Tasmania. *Biogeosciences Discussions*, *14*, 5217–5237. https://doi.org/10.5194/bg-2017-213

Perez, F. F., & Fraga, F. (1987). Association constant of fluoride and hydrogen ions in seawater. *Marine Chemistry*, *21*(2), 161–168. https://doi.org/10.1016/0304-4203(87)90036-3

Rickard, G. J., Behrens, E., & Chiswell, S. M. (2016). CMIP5 Earth system models with biogeochemistry: An assessment for the southwest Pacific Ocean. *Journal of Geophysical Research: Oceans*, *121*, 7857–7879. https://doi.org/10.1002/2016JC011736

Roden, N. P., Shadwick, E. H., Tilbrook, B., & Trull, T. W. (2013). Annual cycle of carbonate chemistry and decadal change in coastal Prydz Bay, East Antarctica. *Marine Chemistry*, *155*, 135–147. https://doi.org/10.1016/j.marchem.2013.06.006

Roden, N. P., Tilbrook, B., Trull, T. W., Virtue, P., & Williams, G. D. (2016). Carbon cycling dynamics in the seasonal sea-ice zone of East Antarctica. *Journal of Geophysical Research: Oceans*, *121*, 8749–8769. https://doi.org/10.1002/2016JC012008

Sarmiento, J. L., & Gruber, N. (2006). *Ocean biogeochemical dynamics*. Princeton, New Jersey: Princeton University Press.

Sasse, T. P., McNeil, B. I., Matear, R. J., & Lenton, A. (2015). Quantifying the influence of $CO_2$ seasonality on future ocean acidification. *Biogeosciences Discussions*, *12*(20), 6017–6031. https://doi.org/10.5194/bgd-12-6017-2015

Shadwick, E. H., Trull, T. W., Thomas, H., & Gibson, J. (2013). Vulnerability of polar oceans to anthropogenic acidification: Comparison of Arctic and Antarctic seasonal cycles. *Scientific Reports*, *3*(1), 2339. https://doi.org/10.1038/srep02339

Sprintall, J., Chereskin, T. K., & Sweeney, C. (2012). High-resolution underway upper ocean and surface atmospheric observations in Drake Passage: Synergistic measurements for climate science. *Oceanography*, *25*(3), 70–81. https://doi.org/10.5670/oceanog.2012.77

Takahashi, T., Sutherland, S. C., Chipman, D. W., Goddard, J. G., & Ho, C. (2014). Climatological distributions of pH, $pCO_2$, total $CO_2$, alkalinity, and $CaCO_3$ saturation in the global surface ocean, and temporal changes at selected locations. *Marine Chemistry*, *164*, 95–125. https://doi.org/10.1016/j.marchem.2014.06.004

Takahashi, T., Sutherland, S. C., Wanninkhof, R., Sweeney, C., Feely, R. A., Chipman, D. W., et al. (2009). Climatological mean and decadal change in surface ocean $pCO_2$, and net sea–air $CO_2$ flux over the global oceans. *Deep-Sea Research Part II: Topical Studies in Oceanography*, *56*(8–10), 554–577. https://doi.org/10.1016/j.dsr2.2008.12.009

Talley, L. D., Feely, R. A., Dickson, A. G., Swift, J. H., Carlson, C. A., Warner, M., et al. (2015). Carbon dioxide, hydrographic, and chemical data obtained during the RVIB Nathaniel B. Palmer Repeat Hydrography Cruises in the Pacific Ocean: GO-SHIP Sections P16S_2014 (20 March–5 May, 2014). Oak Ridge, Tennessee: Carbon Dioxide Information Analysis Center, Oak Ridge National Laboratory, US Department of Energy. https://doi.org/10.3334/CDIAC/OTG.GO_SHIP_P16S_2014

Uppström, L. R. (1974). The boron/chlorinity ratio of deep-sea water from the Pacific Ocean. *Deep Sea Research and Oceanographic Abstracts*, *21*(2), 161–162. https://doi.org/10.1016/0011-7471(74)90074-6

van Heuven, S., Pierrot, D., Rae, J. W. B., Lewis, E., & Wallace, D. W. R. (2011). MATLAB program developed for $CO_2$ system calculations. ORNL/CDIAC-105b. Oak Ridge, Tennessee: Oak Ridge National Laboratory, US Dept. of Energy. https://doi.org/10.3334/CDIAC/otg.CO2SYS_MATLAB_v1.1

Wanninkhof, R. (2014). Relationship between wind speed and gas exchange over the ocean revisited. *Limnology and Oceanography: Methods*, *12*(6), 351–362. https://doi.org/10.4319/lom.2014.12.351

Wanninkhof, R., Johnson, K., Williams, N., Sarmiento, J., Riser, S., Briggs, E., et al. (2016). An evaluation of pH and $NO_3$ sensor data from SOCCOM floats and their utilization to develop ocean inorganic carbon products. A summary of discussions and recommendations of the Carbon Working Group (CWG) of SOCCOM. Available at http://soccom.princeton.edu/sites/default/files/files/CWG_white_paper_March_13_2016.pdf

Wanninkhof, R., Park, G. . H., Takahashi, T., Sweeney, C., Feely, R., Nojiri, Y., et al. (2013). Global Ocean carbon uptake: Magnitude, variability and trends. *Biogeosciences*, *10*(3), 1983–2000. https://doi.org/10.5194/bg-10-1983-2013

Williams, N. L., Feely, R. A., Sabine, C. L., Dickson, A. G., Swift, J. H., Talley, L. D., & Russell, J. L. (2015). Quantifying anthropogenic carbon inventory changes in the Pacific sector of the Southern Ocean. *Marine Chemistry*, *174*, 147–160. https://doi.org/10.1016/j.marchem.2015.06.015

Williams, N. L., Juranek, L. W., Feely, R. A., Johnson, K. S., Sarmiento, J. L., Talley, L. D., et al. (2017). Calculating surface ocean $pCO_2$ from biogeochemical Argo floats equipped with pH: An uncertainty analysis. *Global Biogeochemical Cycles*, *31*, 591–604. https://doi.org/10.1002/2016GB005541